Applied Energy 328 (2022) 120103

Contents lists available at ScienceDirect

Applied Energy

journal homepage: www.elsevier.com/locate/apenergy

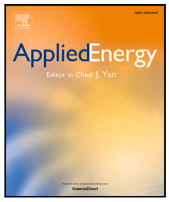

PV–battery-hydrogen plant: Cutting green hydrogen costs through multi-market positioning

Ivan Pavić, Nikolina Čović, Hrvoje Pandžić *

Department of Energy and Power Systems, University of Zagreb Faculty of Electrical Engineering and Computing, Unska 3, Zagreb, 10000, Croatia

ARTICLE INFO

Keywords:
Battery storage
Hydrogen storage
Electrolyzer
Fuel cell
Electricity balancing
Gas grid
Hydrogen grid

ABSTRACT

Integration of renewable energy sources as one of the pillars of the power system decarbonization efforts is making a significant progress. However, large shares of renewables require additional flexibility to keep the system stable. Battery storage was identified as one of the solutions to restore the grid balance in short timeframes, from day-ahead to real time. Currently, the research community is trying to find an adequate technology for longer duration energy storage. Hydrogen, as an energy carrier, appears as a good choice for such task. Apart from hydrogen energy storage potential, it can also be used to implement power-to-gas technology able to mitigate renewable energy curtailment through the process of electrolysis. The produced hydrogen gas can be either used to partially decarbonize the natural gas grids or simply sold as hydrogen fuel.

The main novelty of this paper is the creation of a mathematical model of a renewable power plant coupled with a battery storage and a hydrogen facility for trading in three day-ahead energy markets, i.e. electricity, natural gas and hydrogen, plus in the power balancing market subject to the imbalance settlement mechanism. This approach enables a long-term profitability analysis of different renewable, battery and hydrogen architectures (hydrogen energy storage, power-to-gas and their combination) and their participation in different markets.

The results indicate that the battery energy storage provides balancing services to the transmission system operator almost exclusively, while it never provides balancing for its own imbalance needs, since this option is less financially attractive. The electrolyzer and the fuel cell operate at least one third of the year, depending on the observed case, and often provide a reserve. When considering the hydrogen market, the electrolyzer operates almost the entire year due to lucrative hydrogen prices. Both the battery storage and the hydrogen tank perform arbitrage in the day-ahead market, where the battery optimizes its operation on an hourly basis (short-term) and the hydrogen tank on a daily basis (medium- to long-term).

1. Introduction

To fulfill the Paris Agreement goals, the EU Commission created a set of policy initiatives called the European Green Deal [1], with an overarching aim of making Europe climate neutral by 2050. The energy sector currently generates over 75% of the greenhouse gas emissions in the EU and its decarbonization is crucial to reach the EU's ambitious climate objectives. The power sector is leading the way, where renewable energy sources (RES) integration started two decades ago. Its share has been increasing continuously from 9.6% in 2004 to 19.7% in 2019 [2]. Renewable generation is characterized by variable (both short- and long-term) and uncertain generation, thus requiring an increased power system flexibility [3,4]. One of the potential solutions that emerged in the last couple of years for short-term flexibility is battery energy storage (BES) [5], based on lithium-ion technology [6]. Since lithium-ion batteries operate in timescales of seconds to hours, they are not suitable to shift energy between days, weeks, months, or seasons. Lithium-ion batteries are highly efficient (>85%) [7] and are able to repay their investment cost only with frequent cycling, however, with increasing storage duration their levelized cost of energy (LCOE) significantly increases [8]. Other storage technologies, such as pumped hydro plants, compressed air, or storing energy as fuel (natural gas, hydrogen, methane) are more suitable for medium- to long-term storage applications. As hydrogen energy storage (HES) seems to be the most viable option [9], this paper focuses on combining a BES and a HES with a RES, and maximizes their profit by trading in their respective trading floors, i.e. power, hydrogen, and gas markets.

* Corresponding author.
E-mail address: hrvoje.pandzic@ieee.org (H. Pandžić).

https://doi.org/10.1016/j.apenergy.2022.120103
Received 11 April 2022; Received in revised form 14 September 2022; Accepted 2 October 2022

Nomenclature

Abbreviations

aFRR	Automatic Frequency Restoration Reserve
BES	Battery Energy Storage
BC	Balancing Capacity
BE	Balancing Energy
BG	Balancing Group
CEGH	Central European Gas Hub
CROPEX	Croatian Power Exchange
DAM	Day-ahead Market
EU	European Union
HES	Hydrogen Energy Storage
IDM	Intraday Market
LCOE	Levelized Cost of Energy
P2G	Power-To-Grid
PV	Photovoltaics
RES	Renewable Energy Sources
SOE	State-of-Energy
TSO	Transmission System Operator

Parameters

$\lambda_t^{\mathrm{da,g}}$	Gas DAM price in time period t (€/MWh)
$\lambda_t^{\mathrm{da,h}}$	Hydrogen DAM price in time period t (€/MWh)
$\lambda_t^{\mathrm{da,p}}$	Electricity DAM price in time period t (€/MWh)
$\lambda_t^{\mathrm{d,bc}}$	Downward BC price in time period t (€/MWh)
$\lambda_t^{\mathrm{u,bc}}$	Upward BC price in time period t (€/MWh)
$\lambda_t^{\mathrm{d,be}}$	Downward BE price in time period t (€/MWh)
$\lambda_t^{\mathrm{u,be}}$	Upward BE price in time period t (€/MWh)
$\lambda_t^{\mathrm{d,bg}}$	BG downward imbalance price in time period t (€/MWh)
$\lambda_t^{\mathrm{u,bg}}$	BG upward imbalance price in time period t (€/MWh)
$\lambda_t^{\mathrm{in,g}}$	Energy component of the gas grid tariff in time period t (€/MWh)
$\lambda_t^{\mathrm{in,h}}$	Energy component for injection of the hydrogen grid tariff in time period t (€/MWh)
$\lambda_m^{\mathrm{inm,p}}$	Power component of the electricity grid tariff for injected power in month m (€/MW)
$\lambda_t^{\mathrm{w,h}}$	Energy component for withdrawal of the hydrogen grid tariff in time period t (€/MWh)
$\lambda_t^{\mathrm{w,p}}$	Energy component of the electricity grid tariff in time period t (€/MWh)
$\lambda_m^{\mathrm{wm,p}}$	Power component of the electricity grid tariff for withdrawn power in month m (€/MW)
η^{ch}	BES charging efficiency (%)
η^{dis}	BES discharging efficiency (%)
η_t^{el}	Electrolyzer operation efficiency (%)
η_t^{fc}	Fuel cell operation efficiency (%)
$\eta^{\mathrm{el\_comp}}$	Bus injection compression efficiency (%)
$\eta^{\mathrm{ht\_comp}}$	Hydrogen tank compression efficiency (%)
A^{d}	Portion of activation of downward BC (%)
A^{u}	Portion of activation of upward BC (%)
F_i	Maximum amount of energy that can be charged at a specific BES state of energy breakpoint R_i as a portion of installed BSS capacity (%)
$H^{\mathrm{in,g}}$	Gas grid injection limit (MW)
$H^{\mathrm{in,h}}$	Hydrogen grid injection limit (MW)
H^{ht}	Installed hydrogen tank power (MW)
$H^{\mathrm{w,h}}$	Hydrogen grid withdrawal limit (MW)
I^{s}	Surplus in PV power (%)
I^{l}	Lack in PV power (%)
K_1^{el}, K_2^{el}	Electrolyzer operation linearization parameters
K_1^{fc}, K_2^{fc}	Fuel cell operation linearization parameters
P^{b}	Installed power of BES (MW)
P^{el}	Installed power of electrolyzer (MW)
P^{fc}	Installed power of fuel cell (MW)
P^{in}	Electricity grid injection limit (MW)
P_t^{pv}	Maximum PV output in time period t (MW)
P^{w}	Electricity grid withdrawal limit (MW)
R_i	Capacity of each state of energy battery segment i as a portion of the installed BES capacity (%)
SOE^{b}	BES capacity (MWh)
SOH	Hydrogen tank capacity (MWh)

Variables

Δsoe_t	Amount of energy that can be charged into BES in time period t(%)
θ^{bc}	BC profit (€)
θ^{be}	BE profit (€)
θ^{bg}	Profit from balancing the BG deviations (€)
$\theta^{\mathrm{da,g}}$	Gas DAM profit (€)
$\theta^{\mathrm{da,h}}$	Hydrogen DAM profit (€)
$\theta^{\mathrm{da,p}}$	Electricity DAM profit (€)
$\theta^{\mathrm{grid,p/h/g}}$	Grid tariffs for electricity/hydrogen/gas grid (€)
θ^{hop}	Cost of the hydrogen equipment operation (€)
f_t	Binary variable determining if the fuel cell is operating in time period t
h_t^{ch}	Hydrogen charging to the tank in time period t (MW)
h_t^{dis}	Hydrogen discharging from the tank in time period t (MW)
$h_t^{\mathrm{d,ch}}$	Hydrogen charging to the tank in the worst case of downward reserve activation in time period t (MW)
$h_t^{\mathrm{d,dis}}$	Hydrogen discharging to the tank in the worst case of downward reserve activation in time period t (MW)
$h_t^{\mathrm{d,in,g}}$	Hydrogen injected to the gas grid in the worst case of downward capacity activation in time period t (MW)
$h_t^{\mathrm{d,in,h}}$	Hydrogen injected to the hydrogen grid in the worst case of downward capacity activation in time period t (MW)
$h_t^{\mathrm{d,w,h}}$	Hydrogen withdrawn from the hydrogen grid in the worst case of downward capacity activation in time period t (MW)

$h_t^{d,el}$	Hydrogen produced by the electrolyzer in the worst case of downward reserve activation in time period t (MW)
$h_t^{d,fc}$	Hydrogen used for the fuel cell operation in the worst case of downward reserve activation in time period t (MW)
$h_t^{da,g/h}$	Power traded in gas/hydrogen DAM in time period t (MW)
h_t^{el}	Hydrogen produced by the electrolyzer in time period t (MW)
h_t^{fc}	Hydrogen used for the fuel cell operation in time period t (MW)
$h_t^{in,g}$	Hydrogen injected into the gas grid in time period t (MW)
$h_t^{in,h}$	Hydrogen injected into the hydrogen grid in time period t (MW)
$h_t^{u,ch}$	Hydrogen charging into the tank in the worst case of upward reserve activation in time period t (MW)
$h_t^{u,dis}$	Hydrogen discharging from the tank in the worst case of upward reserve activation in time period t (MW)
$h_t^{u,el}$	Hydrogen produced by the electrolyzer in the worst case of upward reserve activation in time period t (MW)
$h_t^{u,fc}$	Hydrogen used for the fuel cell operation in the worst case of upward reserve activation in time period t (MW)
$h_t^{u,in,g}$	Hydrogen injected into the gas grid in the worst case of upward capacity activation in time period t (MW)
$h_t^{u,in,h}$	Hydrogen injected into the hydrogen grid in the worst case of upward capacity activation in time period t (MW)
$h_t^{u,w,h}$	Hydrogen withdrawn from the hydrogen grid in the worst case of upward capacity activation in time period t (MW)
$h_t^{w,h}$	Hydrogen withdrawn from the hydrogen grid in time period t (MW)
p_t^{ch}	Charging power of the BES in time period t (MW)
p_t^{dis}	Discharge power of the BES in time period t (MW)
$p_t^{d,in}$	Power injected to the power system in the worst case of downward reserve in time period t (MW)
$p_t^{d,w}$	Power withdrawn from the power system in the worst case of downward reserve in time period t (MW)
p_t^{da}	Power traded in the electricity DAM at hour t (MW)
$p_t^{ee,el}$	Total electrical power needed for the electrolyzer operation in time period t (MW)
$p_t^{ee,fc}$	Total electrical power produced by the fuel cell in time period t (MW)
p_t^{el}	Power used for the electrolyzer operation in time period t (MW)
p_t^{fc}	Power produced by the fuel cell in time period t (MW)
$p_t^{i,ch}$	Increased BES charging to provide down reserve in time period t (MW)
$p_t^{i,dis}$	Increased BES discharging to provide up reserve in time period t (MW)
$p_t^{i,el}$	Increased power intake for the electrolyzer operation to provide down reserve in time period t (MW)
$p_t^{i,fc}$	Increased energy generation of the fuel cell to provide up reserve in time period t (MW)
p_t^{in}	Power injected to the power system in time period t (MW)
p_t^{pv}	Power produced by the PV (MW)
$p_t^{r,ch}$	Reduced BES charging for upward reserve in time period t (MW)
$p_t^{r,dis}$	Reduced BES discharging to provide down reserve in time period t (MW)
$p_t^{r,el}$	Reduced power intake for the electrolyzer operation to provide upward reserve in time period t (MW)
$p_t^{r,fc}$	Reduced energy generation of the fuel cell to provide upward reserve in time period t (MW)
$p_t^{u,in}$	Power injected to the power system in the worst case of upward capacity activation in time period t (MW)
$p_t^{u,w}$	Power withdrawn from the power system in the worst case of upward capacity activation in time period t (MW)
p_t^{w}	Power withdrawn from the power system in time period t (MW)
p_m^{inm}	Maximum injected power to the power system in month m (MW)
p_m^{wm}	Maximum withdrawn power from the power system in month m (MW)
$r_t^{d,bc}$	Reserved capacity in the downward direction in time period t (MW)
$r_t^{d,bg}$	BG downward balancing power in time period t (MW)
$r_t^{u,bc}$	Reserved capacity in upward direction in time period t (MW)
$r_t^{u,bg}$	BG upward balancing power in time period t (MW)
soe_t	State of energy of the BES in time period t (MWh)

1.1. Battery energy storage

In this Subsection, we go through different services proposed in literature that a BES can provide to the power system. In the end, we highlight the ones relevant to our paper.

New RES-BES plants are capable of providing flexibility services to the power system [10,11]. Generally, RES plants integrate a behind-the-meter BES to cover their own imbalances. Consequently, different forecasting algorithms lead to different imbalance needs and BES usage and cycling [12]. A BES within a RES-BES plant must also consider energy price forecasts to maximize its revenues [13]. During the BES sizing for minimizing the imbalances, it is important to include all relevant technical limitations affecting the RES-BES real-time operation [14]. It is also important to optimally manage energy flows [15] and employ control strategies to reduce the voltage and frequency fluctuations [16].

$soe_{t,i}$	State of energy of the BES segment i in time period t (MWh)
soh_t	State of energy of the hydrogen tank in time period t (MWh)
w_t	Binary variable determining if the electrolyzer is operating in time period t
x_t^{b}	Binary variable restricting simultaneous BES charging and discharging in time period t
x_t^{h}	Binary variable restricting simultaneous injection to and withdrawal from the hydrogen system in time period t
x_t^{ht}	Binary variable restricting simultaneous hydrogen tank charging and discharging in time period t
x_t^{p}	Binary variable restricting simultaneous injection to and withdrawal from the power system in time period t

A BES can also be efficiently utilized to provide balancing services to the system operators. A standalone BES can provide fast services such as frequency containment reserves [17] or automatic frequency restoration services [18,19]. When providing frequency regulation, the RES-BES plant optimization/control algorithms must incorporate both the RES generation and the frequency regulation forecasts [20]. Provision of fast balancing services entails frequent cycling leading to degradation issues, which can be considered by incorporating a life-cycle model in the profit maximization function [21].

With higher price volatility, a standalone BES can perform a profitable arbitrage at energy markets [22]. However, a BES coupled with an RES can, additionally, shift the RES generation to periods with higher prices, thus providing simultaneously two services [23]. Stacking additional services, as in [24], can even further increase the BES profitability, however, its performance depends on many complex algorithms. E.g., in [25], an artificial intelligence-based algorithm is used to optimize arbitrage, PV generation shifting, and frequency regulation provision of a PV–battery system. Another example can be found in [26], where a BES is used simultaneously for the distributed voltage control and the frequency containment reserve.

The RES-BES combination can also be used within other objects, such as electric vehicle charging stations, to reduce the impact on the grid and to improve the quality of the charging services [27] or smart home arrangements for the provision of multiple services [19]. The literature also proposes RES-BES microgrids either only grid-connected [28] or with islanding capabilities [29]. During the island microgrid operation, the BES must be coordinated with the RES generation, mostly PV, to stabilize the voltage levels [30,31]. The overall power system resilience can be improved with PV-BES plants through their optimal allocation throughout the grid [32]. A BES can be used to re-electrify, or provide black start service after a blackout [33]. An investment in BES can be economically more attractive than network expansions to increase the security of the supply of weakly connected grids [34,35].

The review of the state-of-the-art literature shows a great diversity of services that can be provided by a BES: from RES balancing, balancing services provision, arbitrage, through voltage and resilience, to multiple services stacking in BES standalone options or integrated modes with other objects such as EV charging stations or microgrids. The focus of this paper is on the system-wide services, which means we do not observe grid-specific services such as voltage, islanding, and resilience services. We observe and model a RES-BES facility integrated with a hydrogen facility to provide a wide range of electricity services (RES balancing, system balancing, and arbitrage considering the grid utilization fees) plus energy transfer between different energy vectors, i.e. power, hydrogen, and gas. To the authors' best knowledge, such BES service stacking with a hydrogen facility has not yet been proposed.

1.2. Hydrogen energy storage and power-to-gas facilities

In this subsection, we define the main parts of hydrogen facilities, discuss their potential services provision, costs, and future integration plans. In the end, we define the services considered in this paper.

In general, hydrogen technology solutions are composed of three main parts: hydrogen generation, storage, and utilization. Hydrogen can be generated in multiple ways using processes such as steam reforming and gasification of fossil and non-fossil fuels or processes, such as water electrolysis [36,37]. Natural gas is currently the primary source of hydrogen production (grey hydrogen or blue hydrogen if supported by carbon capture and storage), accounting for around 76% of the global hydrogen production. The rest of the hydrogen is produced mostly from coal (brown hydrogen)—around 23%, while only less than 2% is produced by water electrolysis, i.e. green hydrogen [37]. If the electricity used in electrolysis is generated from RES, such hydrogen is termed green.

Today, hydrogen is mostly stored as gas or liquid in tanks for small-scale mobile and stationary applications [38]. Compressed hydrogen is a viable option for seasonal storage according to [39]. In power systems hydrogen can be utilized for electricity production using either fuel cells or as a fuel in hydrogen-fired gas turbines [37]. In this paper, we focus on modular and clean HES architecture composed of a fuel cell, a compressed hydrogen tank, and an electrolyzer.

The upside of HES is that it can be used both as a short-term and medium- to long-term storage. As far as the short-term storage is concerned, the electrolyzers and fuel cells can ramp up quickly [40] and provide fast ancillary services, such as virtual inertia and frequency regulation [41,42]. Using fuel cells for the RES-production following was proposed in [43,44]. Since there is no loss of hydrogen, there is a high potential for medium- to long-term energy-storing [45,46]. LCOE of such HES increases with storage duration but at a lower gradient as compared to lithium-ion batteries. According to [8], storage durations lower than 13-15 h favor lithium-ion BES, while storage durations over 15 h favor HES. Low cycle efficiency (<40%) of HES is the main drawback to its wider adoption [37]. The existing literature does not focus on the usage of HES for both the short- and the long-term energy storage, its combination with BES nor the provision of a wider range of system-wide services. This paper intends to fill the explored research gap.

The future usage of hydrogen in the power system is expected to be as long-term storage, as well as a clean fuel in the transport sector and industry [37,47], but also as a tool to decarbonize the gas grids [37].

The EU has ambitious plans for hydrogen production, focused on installing 6 GW of renewable-powered electrolyzers by 2025 and 40 GW by 2030. Until 2050 the renewable hydrogen technologies should reach maturity and be deployed at a very large scale [48]. According to [49], the blue hydrogen's LCOE is around 65–70 Eur/MWh, while the green hydrogen's LCOE, produced from otherwise curtailed RES, is around 70 Eur/MWh and around 210 Eur/MWh when produced at an industrial electricity tariff. In [50], the authors report the LCOE for green hydrogen to be around 280, 350, and 475 Eur/MWh in Europe in 2020 when curtailed RES, industrial tariff, and dedicated RES electricity are considered, respectively. Except when free curtailed renewable electricity is used, most of the LCOE comes from the operating costs (75%–90%), predominantly electricity costs [49]. LCOE of blue hydrogen is expected to rise toward 2050 [49], while the LCOE of green hydrogen is to reduce significantly [49,50]. It should be noted that LCOE calculations never take into account the balancing services nor the multi-market arbitrage aspects. Since electricity is the main cost segment, we believe that integration of those services/markets

can significantly improve the profitability of hydrogen production. We pursue this unexplored research avenue in this paper.

Around 3 million km of natural gas transmission pipelines are in operation today around the world, and even greater lengths of distribution pipelines [37]. Hydrogen can be blended into the gas grids in ratios of 5%–20% [51] and can play a significant role in the early stage transition towards hydrogen economy [48]. Some of the natural gas grids can be re-purposed or new dedicated pipelines can be built to transport clean hydrogen [48,51]. The European Network of Transmission System Operators for Gas (ENTSO-G) takes into account hydrogen, along with biomethane, as a natural gas grid decarbonization tool, and they also see themselves as a hydrogen/methane dedicated grid operators [52]. The first step toward a dedicated hydrogen grid, evolved from the natural gas pipelines, is taken by the Dutch government as they plan to have a hydrogen transmission ring through the Netherlands until 2030 [53].

Using RES to produce gas, such as hydrogen, and inject it into the gas grid is termed power-to-gas (P2G) technology [54,55]. P2G is researched in many different forms, from the electricity market participation [56], joint reserve provision with RES [57], to multi-energy market participation, i.e. electricity, natural gas, and hydrogen market [58,59]. The public plans and scientific community see P2G as a service provider to the power system and a decarbonization tool for gas grids. However, there is still a lack of proper long-term analysis to point out whether it is more meaningful to use it for the former or the latter reason. This paper aims at answering this question by creating a model for the profitability of P2G for multiple services and within multiple markets.

1.3. Research focus and contributions

The conducted state-of-the-art literature clearly indicates that both the BES and HES/P2G are seen as attractive decarbonization tools within the smart grid domain [60]. However, the literature is lacking several important points when it comes to the BES and HES/P2G integration into different market structures and, consequently, the profitability of such facilities. These missing points translate into the contribution of this paper. Therefore the contributions of the paper are twofold: development of a comprehensive RES-BES-Hydrogen model for long-term analysis and a detail analysis of such facility using real data as inputs.

The developed comprehensive model covers the following:

- operational scheduling of a PV facility with integrated short- to long-term storage technologies, BES and HES, within a single facility,
- operational scheduling for simultaneous use of an electrolyzer and a fuel cells, where the produced hydrogen can be either fed into the gas/hydrogen network (P2G) or converted back into electricity (HES),
- a multi-market participation (electricity, natural gas, and hydrogen) of the proposed plant with consideration of dynamic prices and balancing services and imbalance penalization in the electricity market,
- a multi-energy framework incorporating the effect of balancing services activation,
- a long-term analysis of operational profitability of different RES-BES–HES/P2G architectures and participation in different energy markets.

This paper provides answers to the following research questions:

- Can HES serve as a short- and/or long-term storage under the current prices?
- Does it complement or overlap with the BES integrated within a RES plant?
- Is it more attractive to use fuel cells or P2G capabilities?
- Which market brings the highest revenues and which subsystems provide the most profitable services?

The rest of the paper is organized as follows. Section 2 explains different technology settings and market architectures examined in this paper. Section 3 formulates a mathematical model that represents the optimal operation of a PV-BES-Hydrogen plant. Section 4 lists and elaborates the input data required to simulate real-world market conditions. Section 5 reports and discusses the results of the conducted case study. Finally, Section 6 concludes the paper and discusses the main findings.

2. Modeling framework

The modeled PV-BES-Hydrogen plant is considered to be built in Croatia, indicating that we observe the European context of harmonized and integrated European-wide energy market.

2.1. PV-BES-hydrogen plant architectures

The hydrogen plant in this paper is coupled with a RES power plant and connected to the electricity grid in all test cases and scenarios. Three hydrogen power plant architectures are considered: HES, P2G, and HES–P2G.

2.1.1. HES

In this architecture the hydrogen is generated, stored, and used only as an energy storage medium for the power system purposes: (RES) balance group balancing, balancing services provision to the Transmission System Operator (TSO) considering both the capacity and activated energy, short-term electricity arbitrage, and long-term electricity arbitrage. It consists of the power part (a RES power plant, a BES facility, an electrical substation, and a connection to the transmission power grid) and the hydrogen part (an electrolyzer, hydrogen storage tanks, and a fuel cell). This architecture is visualized in Fig. 1. The hydrogen storage in this architecture serves as a complementary or competitive technology to BES. The priority of power and hydrogen production solely depends on economic benefits to the facility.

2.1.2. P2G

In the P2G architecture the hydrogen is generated, stored and sold as a fuel either in the national natural gas or the hydrogen market. Its power part is identical to the one in the HES architecture, but the hydrogen part consists of an electrolyzer, a hydrogen tank and a connection to natural gas/hydrogen transmission grids, see Fig. 2. The hydrogen storage in this architecture serves as a green hydrogen generation facility or an energy conversion technology between different energy vectors.

2.1.3. HES-P2G

In this architecture, the hydrogen is generated, stored, and either converted back to electricity or sold as a fuel either at the national natural gas or the hydrogen market. Its power part is identical to the HES/P2G architecture, but the hydrogen part consists of an electrolyzer, hydrogen storage tanks, a fuel cell, and a connection to the natural gas/hydrogen transmission grid, see Fig. 3. The hydrogen storage in this architecture serves as both a complementary/competitive technology to BES and as a hydrogen generation technology or energy conversion technology between different energy vectors.

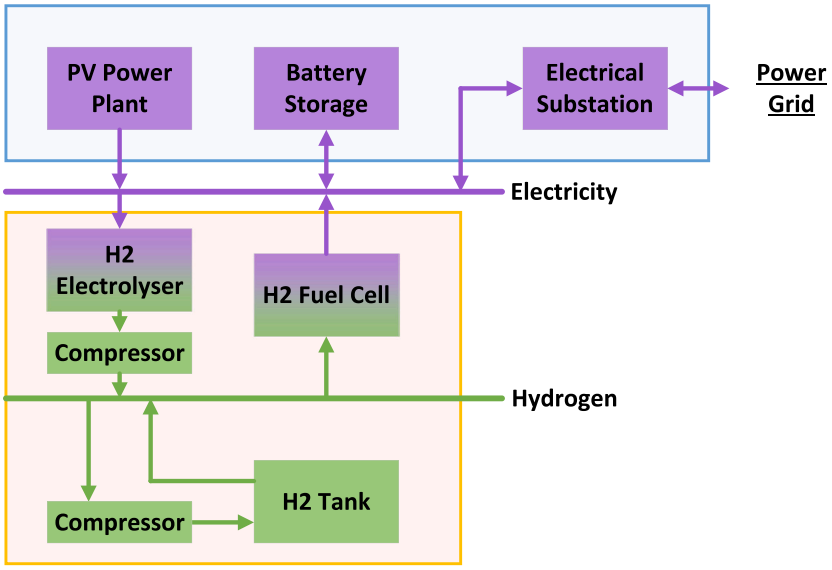

Fig. 1. Hydrogen energy storage architecture.

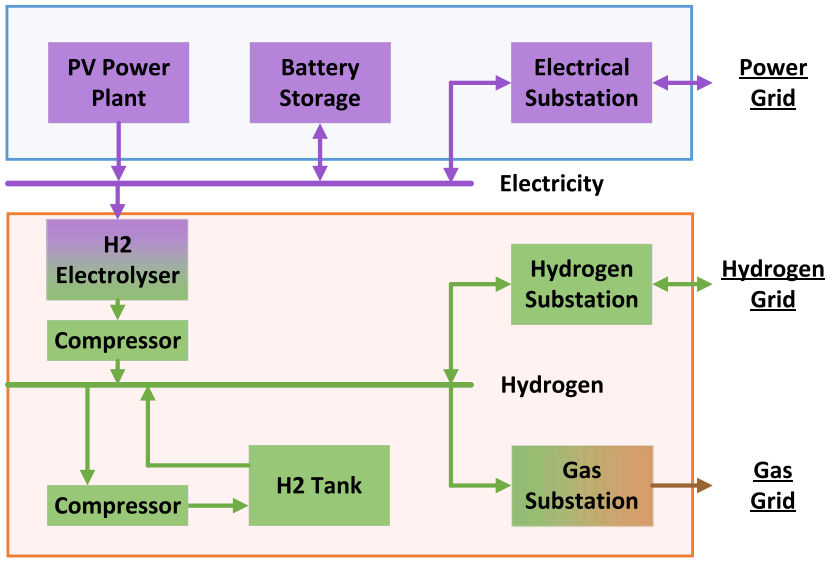

Fig. 2. Power-to-gas architecture.

2.2. Markets and services

As we consider three different energy systems, we observe three wholesale day-ahead markets. Additionally, balancing services in the power system are modeled. Therefore, there are four main markets used in this paper:

1. Wholesale electricity DAM,
2. Balancing services in the power system:
3. Wholesale natural gas DAM,
4. Wholesale hydrogen DAM.

Fig. 4 shows the different roles taken by the PV-BES-Hydrogen plant within this paper. In the wholesale markets, the plant acts as a producer and supplier in the electricity and the hydrogen DAM, while in the gas DAM it acts only as a producer (it cannot withdraw gas and use it within the facility). Additionally, within the power system, the plant is subject to an imbalance settlement mechanism taking responsibility for the deviations from its market position, i.e. it is a balance group manager mitigating its own imbalances toward the TSO. Further, it provides balancing services to the TSO in the balancing services market. Finally, when it comes to physical energy exchange with the grids, it must pay the grid fees for grid usage to all three TSOs acting like any other grid user.

2.2.1. Wholesale electricity market

Electricity markets in Europe operate on several timescales: from the long-term yearly contracts to the short-term DAM and intraday markets (IDM). The DAM poses as the reference market for both the long-term contracts and the IDM. Generally, the DAM markets operate as marginal pricing auctions with gate closure time at noon on the day ahead in all European power exchanges [61]. Such harmonization enabled the integrated Europe-wide market currently covering most European countries. In this paper, Croatian power exchange CROPEX is used to demonstrate the proposed model.

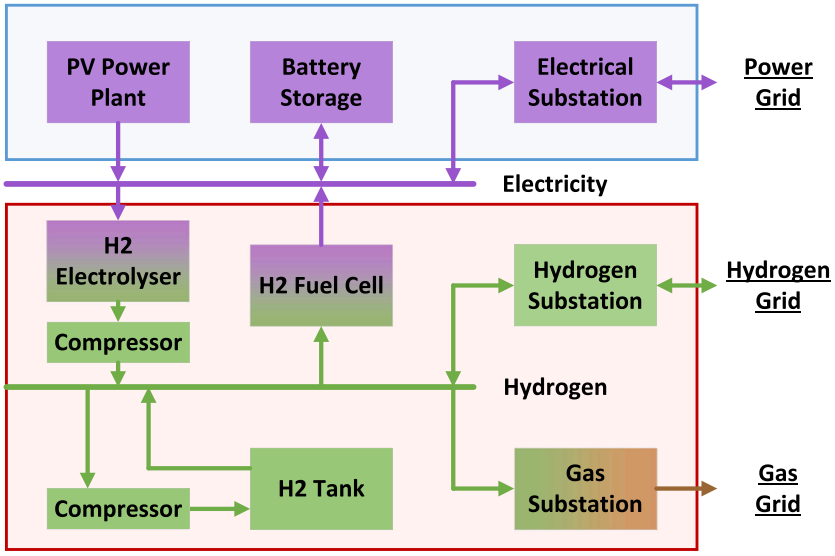

Fig. 3. Hydrogen energy storage + power to gas architecture.

2.2.2. Power system balancing services

Power systems in Europe are organized through a self-dispatch scheme, where each participant (producer, trader, supplier) is responsible for its own market position, i.e. balancing [61]. Each participant must be part of a balancing group (BG) that submits the day-ahead schedules to the TSO. The real-time realizations must match the day-ahead schedules. If a mismatch occurs, the BG must pay for the imbalance to the TSO. Thus, a BG can reserve some of its flexible assets to cover for potential mismatches, otherwise, it pays the imbalance costs. Both of these two options are modeled in this paper. The TSO uses the collected imbalance payments to remunerate the users that provided the balancing services needed to mitigate the system-wide imbalances. Different balancing services can be provided based on the speed of their activation [61]. In this paper, we model the automatic frequency restoration reserve (aFRR), whose providers are paid for both the allocated balancing capacity (BC) in Eur/MW and additionally for the activated balancing energy (BE) in Eur/MWh.

2.2.3. Wholesale gas market

The largest gas exchange, i.e. gas hub, in Europe is TTF in the Netherlands (50 PWh), followed by NBP in the UK (10 PWh). Then, there is a range of mid-volume hubs 0.1–2 PWh (German, Austrian, French, Chech, etc.) and emerging hubs with volumes less than 100 TWh (Romania, Hungary, Denmark, Croatia, etc.). Different products are traded at the EU gas hubs, ranging from intraday/day to monthly/quarterly/season/yearly products where, on average, quarterly and monthly products take the highest share of the trades [62]. The intraday/day-ahead products take an insignificant part of trades on TTF, around 10%–25% on other middle-volume hubs, and the majority of trades on the emerging hubs. Our aim in this paper is to use storage technologies on the gas wholesale market for short-term trading, which is why we focus on the DAM only (long-term markets are less volatile, while intraday markets suffer from liquidity issues). Since the Croatian gas market is small and under development, most of the gas trades in Croatia are made on the Austrian Central European Gas Hub or CEGH, which is the gas market considered in this paper.

2.2.4. Wholesale hydrogen market

Organized hydrogen markets or hydrogen exchanges still do not exist, but according to [63] they must be created along with the hydrogen transmission grid (so-called "hydrogen backbone") to support a new hydrogen economy. The hydrogen market is expected to be halfway between the electricity and the gas market in terms of volatility and temporal dynamics. A future hydrogen exchange, based on the hydrogen backbone and with sufficient diversity of players can operate as a virtual trading point over its entire infrastructure including the international connections, similarly to the gas and electricity exchanges today. One of the important milestones is the launch of a hydrogen price index reflecting the real-market conditions to ease the trading and business planning for future hydrogen market participants. In this paper, we assume future conditions where the hydrogen transmission grid is fully developed with open access to all participants and where the hydrogen exchange operates in a liquid and competitive manner. A new hydrogen index was established in 2021 [64]. It takes into account the production costs and different colors of hydrogen, making it the closest value for hydrogen exchange prices today. Therefore, in this paper, we take this index as a wholesale price of hydrogen at the hydrogen DAM.

2.3. Assumptions

To ease the understanding of the paper we will summarize all the main assumptions regarding the market setup, modeling and inputs:

- All the devices are perfectly controlled and the imbalances can arise only through RES deviations. Average RES deviations and reserve activations are used to reduce the computational burden stemming from the uncertainty modeling.
- CEGH DAM prices were used as gas DAM prices since there is no such market in Croatia. The hydrogen index is used as the hydrogen DAM price since such market does not yet exist. All other similar data are used from the Croatian energy markets.
- Imbalance price is modeled as the worst-case price for both directions based on historical data to ensure the minimization of deviations. All other prices are used as deterministic historical data.
- A linear electrolyzer and fuel cell efficiency curve is used, as explained in Appendix. Hydrogen compression losses are fixed, while the expansion process is lossless. The BSS losses are fixed and the BSS is assumed to be operated under an advanced battery management system minimizing both the losses and degradation. All other losses (such as transforming to a higher voltage) are neglected due to their low effect.

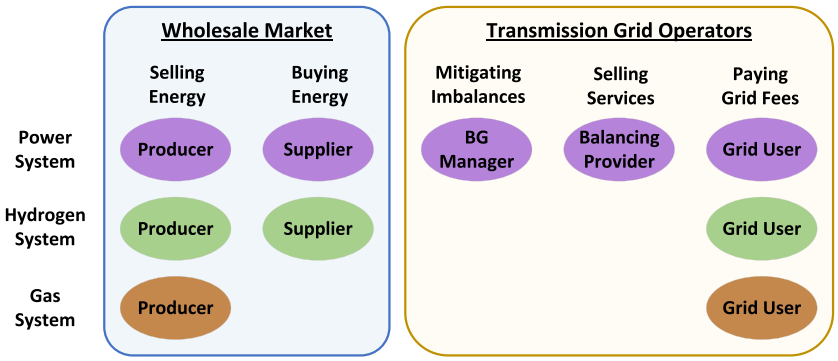

Fig. 4. Different roles of PV-BES-Hydrogen plant.

3. Mathematical model

3.1. Objective function

Objective function (1) maximizes the total profit of the facility stemming from the electricity ($\theta^{\mathrm{da,p}}$), hydrogen ($\theta^{\mathrm{da,h}}$) and gas ($\theta^{\mathrm{da,g}}$) day-ahead markets, electricity balancing capacity (θ^{bc}) and balancing energy (θ^{be}) markets, and profit (i.e. savings) from balancing the deviations of the local PV production (θ^{bg}). It also considers costs (shown as a negative profit) arising from electricity ($\theta^{\mathrm{grid,p}}$), hydrogen ($\theta^{\mathrm{grid,h}}$), and gas ($\theta^{\mathrm{grid,g}}$) grids usage (network fees) as well as from electricity consumption for operation of the hydrogen facility (θ^{hop}). The maximization is performed over a set of variables $\Xi = \left\{ p_t^{\mathrm{da}}, h_t^{\mathrm{in,g}}, h_t^{\mathrm{in,h}}, h_t^{\mathrm{w,h}}, r_t^{\mathrm{u,bc}}, r_t^{\mathrm{d,bc}}, p_t^{\mathrm{pv}}, r_t^{\mathrm{d,bg}}, r_t^{\mathrm{u,bg}} \right\}$.

$$\max_{\Xi} \ \theta^{\mathrm{da,p}} + \theta^{\mathrm{da,h}} + \theta^{\mathrm{da,g}} + \theta^{\mathrm{bc}} + \theta^{\mathrm{be}} + \theta^{\mathrm{bg}} - \theta^{\mathrm{grid,p}} - \theta^{\mathrm{grid,h}} - \theta^{\mathrm{grid,g}} - \theta^{\mathrm{hop}} \quad (1)$$

Profit in the electricity DAM (2) is obtained by selling or purchasing energy $p_t^{\mathrm{da}} \cdot \Delta t$ at price $\lambda_t^{\mathrm{p,da}}$. Equivalently, in (3) energy sold in the hydrogen DAM ($h_t^{\mathrm{da,h}} \cdot \Delta t$) brings income proportional to the hydrogen market price $\lambda_t^{\mathrm{h,da}}$. Profit from selling hydrogen ($h_t^{\mathrm{da,g}} \cdot \Delta t$) in the gas DAM is calculated in (4).

$$\theta^{\mathrm{da,p}} = \sum_t p_t^{\mathrm{da}} \cdot \Delta t \cdot \lambda_t^{\mathrm{da,p}} \quad (2)$$

$$\theta^{\mathrm{da,h}} = \sum_t h_t^{\mathrm{da,h}} \cdot \Delta t \cdot \lambda_t^{\mathrm{da,h}} \quad (3)$$

$$\theta^{\mathrm{da,g}} = \sum_t h_t^{\mathrm{da,g}} \cdot \Delta t \cdot \lambda_t^{\mathrm{da,g}} \quad (4)$$

Eq. (5) calculates the profit from providing BC in both the upward ($r_t^{\mathrm{u,bc}}$) and downward ($r_t^{\mathrm{d,bc}}$) directions. While providing BC always results in positive revenue, participating in the BE market may result in a negative revenue when providing the down reserve, see (6). For simplicity and due to lack of data, the BE activation is given as a percentage ($A^{\mathrm{u}}, A^{\mathrm{d}}$) of the reserved BC in each direction, where the percentage was calculated from historic data.

$$\theta^{\mathrm{bc}} = \sum_t r_t^{\mathrm{u,bc}} \cdot \lambda_t^{\mathrm{u,bc}} + \sum_t r_t^{\mathrm{d,bc}} \cdot \lambda_t^{\mathrm{d,bc}} \quad (5)$$

$$\theta^{\mathrm{be}} = \sum_t A^{\mathrm{u}} \cdot \Delta t \cdot r_t^{\mathrm{u,bc}} \cdot \lambda_t^{\mathrm{u,be}} - \sum_t A^{\mathrm{d}} \cdot \Delta t \cdot r_t^{\mathrm{d,bc}} \cdot \lambda_t^{\mathrm{d,be}} \quad (6)$$

Profit from deviating from the forecasted PV production is given in (7). Deviation in the PV production is assumed to be constant in each direction and equal to a percentage of the PV production for both the underproduction, i.e. lack of output (I^{l}, and overproduction, i.e. surplus output (I^{s}). These percentages represent an average PV forecast error. When deviations occur, it is possible to mitigate them fully by employing controllable units (BES, electrolyzer, fuel cell) or waiting for the imbalance settlement with a partially or fully unbalanced portfolio of the BG. If the BG is unbalanced in real-time, it will pay or be paid for the imbalance energy at the imbalance settlement price $\lambda_t^{\mathrm{u,bg}}$ or $\lambda_t^{\mathrm{d,bg}}$, as calculated in (7).

In case of PV overproduction (BG injects into the grid more power than planned), it is possible to reduce the deviation by increasing the electricity consumption or decreasing the production of controllable units, which is accounted for by variable $r_t^{\mathrm{d,bg}}$, which represents the BG downward balancing power. If the BG still has a surplus of energy, it must sell it at price $\lambda_t^{\mathrm{d,bg}}$, which acts as the down balancing revenue. That price is usually lower than the DAM price for a specific hour, which means that imbalance bears some lost-opportunity costs.

In case of PV underproduction (BG injects less power than planned), the deviation can be mitigated by increasing the electricity production or decreasing the electricity consumption of controllable units, given with variable $r_t^{\mathrm{u,bg}}$, which represents the BG upward balancing power. If there is still a shortage after this balancing (or such balancing is for some reason highly nonprofitable), it is penalized at price $\lambda_t^{u,bg}$. That price is usually higher than the DAM price, which means that imbalance again bears some lost-opportunity costs.

Errors in the PV forecast, in reality, may be greater or lower than the average assumed by coefficients I^{s} and I^{l}, which denote surplus and lack in the PV production, respectively. Coefficients A^{u} and A^{d} indicate the extent to which the imbalance caused by an inaccurate forecast is resolved locally. In case of coefficients A^{u} or A^{d} are equal to one, it is possible to solve only the average imbalance. To make the model robust for higher deviations, coefficients A^{u} and A^{d} may be set to values lower than 1.

$$\theta^{\mathrm{bg}} = \sum_t (I^{\mathrm{s}} \cdot p_t^{\mathrm{pv}} - A^{\mathrm{d}} \cdot r_t^{\mathrm{d,bg}}) \cdot \Delta t \cdot \lambda_t^{\mathrm{d,bg}} - \sum_t (I^{\mathrm{l}} \cdot p_t^{\mathrm{pv}} - A^{\mathrm{u}} \cdot r_t^{\mathrm{u,bg}}) \cdot \Delta t \cdot \lambda_t^{\mathrm{u,bg}} \quad (7)$$

The considered facility is connected to three grids and for each injection/withdrawal, it must pay a specific grid tariff. Tariff fees for the power grid are calculated in (8), for the hydrogen grid in (9), and for the gas grid in (10). The withdrawn electricity is paid both per energy and power component, while the injected electricity is paid per power component only. The power component is calculated on a monthly basis [65]. The grid tariff per energy component must be paid for both injections and withdrawals to/from both the hydrogen and gas grids [66].

$$\theta^{\mathrm{grid,p}} = \sum_t (p_t^{\mathrm{w}} \cdot \Delta t \cdot \lambda_t^{\mathrm{w,p}}) + \sum_m (p_m^{\mathrm{wm}} \cdot \lambda_m^{\mathrm{wm,p}} + p_m^{\mathrm{inm}} \cdot \lambda_m^{\mathrm{inm,p}}) \quad (8)$$

$$\theta^{\mathrm{grid,h}} = \sum_t (h_t^{\mathrm{w,h}} \cdot \Delta t \cdot \lambda_t^{\mathrm{w,h}}) + \sum_t (h_t^{\mathrm{in,h}} \cdot \Delta t \cdot \lambda_t^{\mathrm{in,h}}) \quad (9)$$

$$\theta^{\mathrm{grid,g}} = \sum_t h_t^{\mathrm{in,g}} \cdot \Delta t \cdot \lambda_t^{\mathrm{in,g}} \quad (10)$$

To operate hydrogen compressors, electrical energy must be consumed and purchased in the electricity DAM:

$$\theta^{\mathrm{hop}} = \sum_t (\eta^{\mathrm{el\_comp}} \cdot h_t^{\mathrm{el}} + \eta^{\mathrm{ht\_comp}} \cdot h_t^{\mathrm{ch}}) \cdot \Delta t \cdot \lambda_t^{\mathrm{da,p}} \quad (11)$$

3.2. Electrical power constraints

Power-related constraints given in this subsection are grouped into the main, the BES, the electrolyzer, and the fuel cell constraints.

3.2.1. Main power constraints

Power generated from the PV at each time period (p_t^{pv}) is limited to the maximum available PV production (P_t^{pv}):

$$p_t^{\mathrm{pv}} \le P_t^{\mathrm{pv}}, \quad \forall t \tag{12}$$

Electricity DAM bid (p_t^{da}) is determined in (13) by the amount of discharged and charged energy from the BES (p_t^{dis} and p_t^{ch}), electricity produced by the PV (p_t^{pv}), electricity consumed by the electrolyzer (p_t^{el}), and electricity produced by the fuel cell (p_t^{fc}). All the mentioned values are given as power in MW, and therefore to convert it to energy, their sum is multiplied with time period Δt in (2) which is equal to one hour in today's markets.

$$p_t^{\mathrm{da}} = p_t^{\mathrm{dis}} - p_t^{\mathrm{ch}} + p_t^{\mathrm{pv}} - p_t^{\mathrm{el}} + p_t^{\mathrm{fc}}, \quad \forall t \tag{13}$$

BC in the upward direction ($r_t^{\mathrm{u,bc}}$), as well as the upward BG balancing power ($r_t^{\mathrm{u,bg}}$), can be obtained by reducing the charging ($p_t^{\mathrm{r,ch}}$) and/or by increasing the discharging ($p_t^{\mathrm{i,dis}}$) of the BES, by reducing the hydrogen production of the electrolyzer ($p_t^{\mathrm{r,el}}$) and/or by increasing the electricity production of the fuel cell ($p_t^{\mathrm{i,fc}}$), as given in (14). Similarly, BC in the downward direction ($r_t^{\mathrm{d,bc}}$) and the downward BG balancing power ($r_t^{\mathrm{d,bg}}$) used to mitigate the PV overproduction deviations can be achieved by reducing the discharging ($p_t^{\mathrm{r,dis}}$) or increasing the charging ($p_t^{\mathrm{i,dis}}$) of the BES, by increasing the hydrogen production by the electrolyzer ($p_t^{\mathrm{r,el}}$), and by decreasing the electricity production of the fuel cell ($p_t^{\mathrm{i,fc}}$), as given in (15). In the following text we use a joint term when referring to ($r_t^{\mathrm{u,bc}} + r_t^{\mathrm{u,bg}}$) — up reserve, and a joint term when referring to ($r_t^{\mathrm{d,bc}} + r_t^{\mathrm{d,bg}}$) — down reserve.

$$r_t^{\mathrm{u,bc}} + r_t^{\mathrm{u,bg}} = p_t^{\mathrm{r,ch}} + p_t^{\mathrm{i,dis}} + p_t^{\mathrm{r,el}} + p_t^{\mathrm{i,fc}}, \quad \forall t \tag{14}$$

$$r_t^{\mathrm{d,bc}} + r_t^{\mathrm{d,bg}} = p_t^{\mathrm{r,dis}} + p_t^{\mathrm{i,ch}} + p_t^{\mathrm{i,el}} + p_t^{\mathrm{r,fc}}, \quad \forall t \tag{15}$$

The electricity bus balance needs to be satisfied in all cases of BC activations and PV productions (including the forecast errors). Therefore, three cases of the impact on the electrical power system are presented—the average (expected) one, the worst case in the upward direction, and the worst case in the downward direction.

In the average case, given in (16), it is assumed that the activated BC, i.e. balancing energy, is a certain percentage ($A^{\mathrm{u}}, A^{\mathrm{d}}$) of the reserved BC. Likewise, it is assumed that a certain percentage ($A^{\mathrm{u}}, A^{\mathrm{d}}$) of the reserved power for the BG balancing is utilized. Eq. (17) represents the busbar balance in the worst *injection* case where a full activation of the upward BC and maximum PV surplus considering the downward BG balancing power is assumed. The opposite is modeled in (18), where the worst *withdrawal* case happens. Here, the full activation of the downward BC and maximum PV underestimation considering the upward BG balancing power is assumed.

$$\begin{aligned} &p_t^{\mathrm{da}} + A^{\mathrm{u}} \cdot r_t^{\mathrm{u,bc}} - A^{\mathrm{d}} \cdot r_t^{\mathrm{d,bc}} + A^{\mathrm{u}} \cdot r_t^{\mathrm{u,bg}} - \\ &I^{\mathrm{l}} \cdot p_t^{\mathrm{pv}} - A^{\mathrm{d}} \cdot r_t^{\mathrm{d,bg}} + I^{\mathrm{s}} \cdot p_t^{\mathrm{pv}} = p_t^{\mathrm{in}} - p_t^{\mathrm{w}}, \quad \forall t \end{aligned} \tag{16}$$

$$p_t^{\mathrm{da}} + r_t^{\mathrm{u,bc}} - r_t^{\mathrm{d,bg}} + P_t^{\mathrm{pv}} - p_t^{\mathrm{pv}} = p_t^{\mathrm{u,in}} - p_t^{\mathrm{u,w}}, \quad \forall t \tag{17}$$

$$p_t^{\mathrm{da}} - r_t^{\mathrm{d,bc}} + r_t^{\mathrm{u,bg}} - p_t^{\mathrm{pv}} = p_t^{\mathrm{d,in}} - p_t^{\mathrm{d,w}}, \quad \forall t \tag{18}$$

Eqs. (19) and (20) set the limits for downward and upward BG balancing power variables $r_t^{\mathrm{d,bg}}$ and $r_t^{\mathrm{u,bg}}$, taking into account average PV forecast errors I^{s} and I^{l} and BG activation coefficients A^{u} and A^{d}. They state that the BG reserved power multiplied with the activation coefficient must be lower or equal to the average PV forecast error. It means that the power can be reserved only to cover the imbalances and not to manipulate the imbalance settlement mechanism. Otherwise, it could happen, for example, that the value of $r_t^{\mathrm{u,bg}}$ is intentionally increased to generate income.

$$A^{\mathrm{d}} \cdot r_t^{\mathrm{d,bg}} \le I^{\mathrm{s}} \cdot p_t^{\mathrm{pv}}, \quad \forall t \tag{19}$$

$$A^{\mathrm{u}} \cdot r_t^{\mathrm{u,bg}} \le I^{\mathrm{l}} \cdot p_t^{\mathrm{pv}}, \quad \forall t \tag{20}$$

At all times, the power withdrawn from the grid needs to be lower than P^{w}, as in (21), while the power injected into the grid needs to be lower than P^{in}, as in (22). Injections and withdrawals cannot happen at the same time, which is constrained by binary variables $x^{\mathrm{i,p}}$. These constraints need to be valid in the case of average reserve activation and average deviations from the predicted PV production ($i = \emptyset$), as well as for the worst-case activations/deviations in the upward ($i = u$) and downward directions ($i = d$).

$$p_t^{\mathrm{i,w}} \le P^{\mathrm{w}} \cdot \left(1 - x^{\mathrm{i,p}}\right), \quad \forall t, i \in \{\emptyset, u, d\} \tag{21}$$

$$p_t^{\mathrm{i,in}} \le P^{\mathrm{in}} \cdot x^{\mathrm{i,p}}, \quad \forall t, i \in \{\emptyset, u, d\} \tag{22}$$

Eqs. (23) and (24) calculate the maximum withdrawn (p_m^{wm}) and injected power (p_m^{inm}) within one month. This information is needed to calculate the cost of the monthly power-related grid tariffs used in (8).

$$p_t^{\mathrm{w}} \le p_m^{\mathrm{wm}}, \quad \forall m, t \tag{23}$$

$$p_t^{\mathrm{in}} \le p_m^{\mathrm{inm}}, \quad \forall m, t \tag{24}$$

3.2.2. Battery energy storage constraints

Charging and discharging powers are limited by the BES installed power P^{b} in (25) and (26). Furthermore, those processes cannot happen concurrently, which is constrained by binary variable x_t^{b}.

$$p_t^{\mathrm{ch}} \le x_t^{\mathrm{b}} \cdot P^{\mathrm{b}}, \quad \forall t \tag{25}$$

$$p_t^{\mathrm{dis}} \le (1 - x_t^{\mathrm{b}}) \cdot P^{\mathrm{b}}, \quad \forall t \tag{26}$$

Provision of BC is achieved by altering the charging and discharging of the BES given by (27)–(32). The upward direction can be procured by reduced charging ($p_t^{\mathrm{r,ch}}$) or by increased discharging ($p_t^{\mathrm{i,dis}}$), which cannot happen simultaneously ($x_t^{\mathrm{u,b}}$). If the BES is being charged, the charging power can be reduced so it terminates the charging process, which is modeled in (27). The resulting charging power after the reduction in (28) is limited by the installed power P^{b} as well. On the other hand, the discharge power can be increased up to the amount of the installed power P^{b} given in (29). It must be considered whether the BES is already being discharged in the moment of the upward reserve activation. If so, the amount of possible increase in the discharge will be equal to the difference between the installed power P^{b} and the current discharging power p_t^{dis}. Binary variable $x_t^{\mathrm{u,b}}$ means that the reduction of charging and increase of discharging cannot happen simultaneously. This means that at some time period t, it is necessary to reduce charging completely to allow for an increase in discharge. In such case, the binary variable in the constraint (28) will be equal to 0, $p_t^{\mathrm{r,ch}}$ will be equal to p_t^{ch}, and $p_t^{\mathrm{i,dis}}$ can be set to a certain amount that satisfies (29). Eqs. (30)–(32) are analogous to the ones just described, but for the downward reserves. In that case the BES can increase its charging ($p_t^{\mathrm{i,ch}}$) or decrease its discharging ($p_t^{\mathrm{r,dis}}$). These two actions cannot happen concurrently, which is constrained by binary variable $x_t^{\mathrm{d,b}}$. Constraints (27)–(32) are visualized in Fig. 5. The assumed capacity of each is 25 MW (wide gray bars). Colored bars show the DAM bids, while arrows indicate flexibility that can be offered to the system according to (14) and (15).

$$p_t^{\mathrm{r,ch}} \le p_t^{\mathrm{ch}}, \quad \forall t \tag{27}$$

$$p_t^{\mathrm{ch}} - p_t^{\mathrm{r,ch}} \le x_t^{\mathrm{u,b}} \cdot P^{\mathrm{b}}, \quad \forall t \tag{28}$$

$$p_t^{\mathrm{i,dis}} \le \left(1 - x_t^{\mathrm{u,b}}\right) \cdot P^{\mathrm{b}} - p_t^{\mathrm{dis}}, \quad \forall t \tag{29}$$

$$p_t^{\mathrm{r,dis}} \le p_t^{\mathrm{dis}}, \quad \forall t \tag{30}$$

$$p_t^{\mathrm{i,ch}} \le \left(1 - x_t^{\mathrm{d,b}}\right) \cdot P^{\mathrm{b}} - p_t^{\mathrm{ch}}, \quad \forall t \tag{31}$$

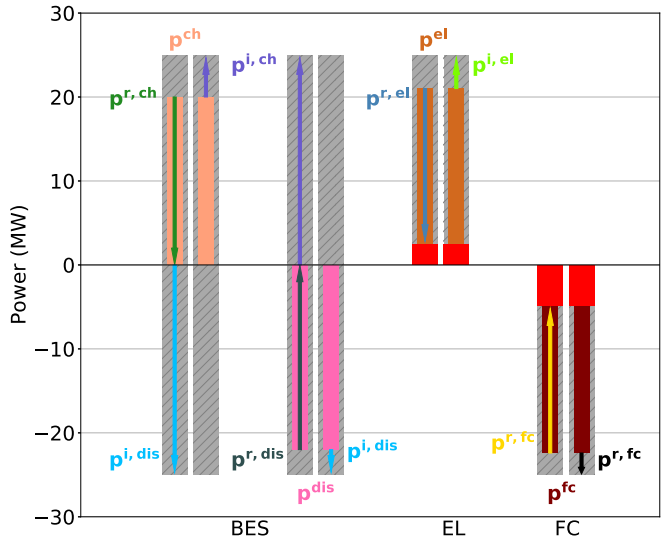

Fig. 5. Visualization of the reserve provision quantities by the BES, the electrolyzer (EL) and the fuel cell (FC).

$$p_t^{\text{dis}} - p_t^{\text{r,dis}} \le x_t^{\text{d,b}} \cdot P^{\text{b}}, \quad \forall t \tag{32}$$

State-of-energy (SOE) of the BES (denoted by variable soe_t) always needs to be higher than zero and lower than the installed BES energy capacity SOE^{b} as in (33). Note that in our formulation we refer to the SOE as the net (usable) BES capacity, which is usually lower than the gross (total) BES capacity. In case when the BES participates in reserve provision, it must have sufficient energy available for this purpose. The worst-case for both the upward and downward reserve provision is when the entire reserved capacity is activated. It is, therefore, necessary for the BES to have a secured capacity that can enable the provision of reserves in the worst case in both directions, which is modeled in (34) and (35). Eq. (36) controls the average reserve activations based on the SOE at the previous time period and the amount of energy charged/discharged into/from the BES at time period t. The charged and discharged energy includes the energy traded in the DAM, along with the activated reserve energy.

$$0 \le soe_t \le SOE^{\text{b}}, \quad \forall t \tag{33}$$

$$soe_{t-1} + (p_t^{\text{ch}} - p_t^{\text{r,ch}}) \cdot \eta^{\text{ch}} \cdot \Delta t \; - (p_t^{\text{dis}} + p_t^{\text{i,dis}}) \cdot \Delta t / \eta^{\text{dis}} \ge 0, \quad \forall t \tag{34}$$

$$soe_{t-1} + (p_t^{\text{ch}} + p_t^{\text{i,ch}}) \cdot \eta^{\text{ch}} \cdot \Delta t \; - (p_t^{\text{dis}} - p_t^{\text{r,dis}}) \cdot \Delta t / \eta^{\text{dis}} \le SOE^{\text{b}}, \quad \forall t \tag{35}$$

$$soe_t = soe_{t-1} + (p_t^{\text{ch}} - A^{\text{u}} \cdot p_t^{\text{r,ch}} + A^{\text{d}} \cdot p_t^{\text{i,ch}}) \cdot \eta^{\text{ch}} \cdot \Delta t$$
$$-(p_t^{\text{dis}} - A^{\text{d}} \cdot p_t^{\text{r,dis}} + A^{\text{u}} \cdot p_t^{\text{i,dis}}) \cdot \Delta t / \eta^{\text{dis}}, \quad \forall t \tag{36}$$

Authors in [67] present an accurate model of the BES charging process, (37)–(40), where the reduced charging power ability at higher SOE is considered. This is the model employed in the following equations, however, for details please refer to [67].

$$soe_t = \sum_{i=1}^{I-1} soe_{t,i}, \quad \forall t \tag{37}$$

$$soe_{t,i} = R_{i+1} - R_i, \quad \forall t, i \tag{38}$$

$$\Delta soe_t = F_1 + \sum_{i=1}^{I-1} \frac{F_{i+1} - F_i}{R_{i+1} - R_i} \cdot soe_{t-1,i}, \quad \forall t \tag{39}$$

$$p_t^{\text{ch}} + p_t^{\text{i,ch}} \le \Delta soe_t / \eta^{\text{ch}}, \quad \forall t \tag{40}$$

3.2.3. Electrolyzer constraints

Eqs. (41) and (42) represent the limits on minimum and maximum power of the electrolyzer. When it operates (indicated by binary variable w_t), there is a technical minimum of 10% of the installed power capacity P^{el} that must be met [68]. The electrolyzer can provide reserves by reducing or increasing its electricity consumption, i.e. hydrogen output. Constraints (43) and (44) are analogous to the BES ones for the upward reserve provision, (27)–(29), with an additional need to ensure that the technical minimum requirements are still met in (43) when reducing the electricity consumption of the electrolyzer. The mechanics of the electrolyzer constraints are given in Fig. 5.

$$p_t^{\text{el}} \ge 0.1 \cdot P^{\text{el}} \cdot w_t, \quad \forall t \tag{41}$$

$$p_t^{\text{el}} \le P^{\text{el}} \cdot w_t, \quad \forall t \tag{42}$$

$$p_t^{\text{r,el}} \le p_t^{\text{el}} - 0.1 \cdot P^{\text{el}} \cdot w_t, \quad \forall t \tag{43}$$

$$p_t^{\text{i,el}} \le P^{\text{el}} \cdot w_t - p_t^{\text{el}}, \quad \forall t \tag{44}$$

3.2.4. Fuel cell constraints

Fuel cell constraints (45) and (46) are analogous to the ones for the electrolyzer. The only difference is in the technical minimum constraint, which for the fuel cell is 20% of the installed capacity [69–71]. Likewise, reserve constraints (47) and (48) are analogous to the BES ones for the downward reserve provision (30) and (32). The mechanics of the fuel cell constraints are also given in Fig. 5.

$$p_t^{\text{fc}} \ge 0.2 \cdot P^{\text{fc}} \cdot f_t, \quad \forall t \tag{45}$$

$$p_t^{\text{fc}} \le P^{\text{fc}} \cdot f_t, \quad \forall t \tag{46}$$

$$p_t^{\text{r,fc}} \le p_t^{\text{fc}} - 0.2 \cdot P^{\text{fc}} \cdot f_t, \quad \forall t \tag{47}$$

$$p_t^{\text{i,fc}} \le P^{\text{fc}} \cdot f_t - p_t^{\text{fc}}, \quad \forall t \tag{48}$$

3.3. Electricity — Hydrogen interface constraints

3.3.1. Electrolyzer hydrogen generation

Constraints describing operation of the electrolyzer connect the hydrogen and the power system. To produce h_t^{el} amount of hydrogen, p_t^{ee} electrical energy is needed, including the electrolyzer efficiency η_t^{el}. However, since this efficiency changes with the operating point of the electrolyzer, i.e. it is a function of p_t^{ee}, it is necessary to linearize constraint (49). The resulting linear constraint (50) is obtained upon the linearization procedure provided in Appendix.

$$h_t^{\text{el}} = p_t^{\text{ee,el}} \cdot \eta_t^{\text{el}}, \quad \forall t \tag{49}$$

$$h_t^{\text{el}} = K_1^{el} \cdot p_t^{\text{ee,el}} + K_2^{el} \cdot P^{\text{el}} \cdot w_t, \quad \forall t \tag{50}$$

To take into account uncertainties that may impact the hydrogen system, three variants of hydrogen production are modeled. They differ in the amount of electricity (p_t^{ee}) used for hydrogen production, which depends on the amount of activated reserves in the power system. Therefore, Eq. (50) is replaced with (51)–(53). When the average activation of reserves in the power system occurs, the amount of hydrogen h_t^{el} is produced, as given in (51). Less hydrogen ($h_t^{\text{u,el}}$) is produced when the most upward reserve is activated as in (52). On the contrary, when the highest possible downward reserve is activated, more hydrogen ($h_t^{\text{d,el}}$) than in the average case is produced, as modeled in (53).

$$h_t^{\text{el}} = K_1^{\text{el}} \cdot (p_t^{\text{el}} + A^{\text{d}} \cdot p_t^{\text{i,el}} - A^{\text{u}} \cdot p_t^{\text{r,el}}) + \; K_2^{\text{el}} \cdot P^{\text{el}} \cdot w_t, \forall t \tag{51}$$

$$h_t^{\text{u,el}} = K_1^{\text{el}} \cdot (p_t^{\text{el}} - p_t^{\text{r,el}}) + K_2^{\text{el}} \cdot P^{\text{el}} \cdot w_t, \quad \forall t \tag{52}$$

$$h_t^{\text{d,el}} = K_1^{\text{el}} \cdot (p_t^{\text{el}} + p_t^{\text{i,el}}) + K_2^{\text{el}} \cdot P^{\text{el}} \cdot w_t, \quad \forall t \tag{53}$$

3.3.2. Fuel cell hydrogen consumption

In the fuel cell, a process opposite to that in the electrolyzer occurs. Since the efficiency of a fuel cell also depends on its operating power as with an electrolyzer, constraint (54) is nonlinear. Analogously to the electrolyzer counterpart constraint, linear Eq. (55) is obtained after linearization.

$$h_t^{\text{fc}} = p_t^{\text{ee,fc}} / \eta_t^{\text{fc}}, \quad \forall t \tag{54}$$

$$h_t^{\text{fc}} = K_1^{\text{fc}} \cdot p_t^{\text{ee,fc}} + K_2^{\text{fc}} \cdot P^{\text{fc}} \cdot f_t, \quad \forall t \tag{55}$$

Again, the amount of activated reserve may impact the operation of the fuel cell. Thus, (55) is replaced with (56)–(58). In the fuel cell, hydrogen is treated as a fuel, and given the amount of reserve required from the power system, the required amount of hydrogen is determined. Eq. (56) represents the case when average reserve activation occurs, while (57) and (58) cover the worst cases of upward and downward reserve activations. As opposed to the electrolyzer-related constraints, the amount of hydrogen in the case of the worst upward reserve activation ($h_t^{\mathrm{u,fc}}$) is higher than in the average case (h_t^{fc}). Contrary, in case of the worst downward reserve, the amount ($h_t^{\mathrm{d,fc}}$) is lower than in the average case.

$$h_t^{\mathrm{fc}} = K_1^{\mathrm{fc}} \cdot (p_t^{\mathrm{fc}} + A^{\mathrm{d}} \cdot p_t^{\mathrm{i,fc}} - A^{\mathrm{u}} \cdot p_t^{\mathrm{r,fc}}) + K_2^{\mathrm{fc}} \cdot P^{\mathrm{fc}} \cdot f_t, \quad \forall t \tag{56}$$

$$h_t^{\mathrm{u,fc}} = K_1^{\mathrm{fc}} \cdot (p_t^{\mathrm{fc}} + p_t^{\mathrm{i,fc}}) + K_2^{\mathrm{fc}} \cdot P^{\mathrm{fc}} \cdot f_t, \quad \forall t \tag{57}$$

$$h_t^{\mathrm{d,fc}} = K_1^{\mathrm{fc}} \cdot (p_t^{\mathrm{fc}} - p_t^{\mathrm{r,fc}}) + K_2^{\mathrm{fc}} \cdot P^{\mathrm{fc}} \cdot f_t, \quad \forall t \tag{58}$$

3.4. Hydrogen constraints

3.4.1. Main hydrogen constraints

Eq. (59) models the amount of hydrogen offered in the DAM ($h_t^{\mathrm{da,h}}$) as the difference between the injections of hydrogen ($h_t^{\mathrm{in,h}}$) and its withdrawals ($h_t^{\mathrm{w,h}}$). In the case of trading in the gas DAM, hydrogen can only be injected and sold, as given by Eq. (60).

$$h_t^{\mathrm{da,h}} = h_t^{\mathrm{in,h}} - h_t^{\mathrm{w,h}}, \quad \forall t \tag{59}$$

$$h_t^{\mathrm{da,g}} = h_t^{\mathrm{in,g}}, \quad \forall t \tag{60}$$

Analogous to the electric power system, in the hydrogen system, the busbar balance must be preserved regardless of the amount of reserve activated in the electric power system. In case the average reserve is activated, (61) must be valid. In case of the worst upward activation given in (62), when it is necessary to increase the amount of electricity in the system, hydrogen consumption for the fuel cell operation increases and hydrogen production from the electrolyzer decreases. Exactly the opposite happens in the case of the worst downward reserve activation given in (63).

$$h_t^{\mathrm{el}} - h_t^{\mathrm{fc}} + h_t^{\mathrm{dis}} - h_t^{\mathrm{ch}} = h_t^{\mathrm{in,h}} + h_t^{\mathrm{in,g}} - h_t^{\mathrm{w,h}}, \quad \forall t \tag{61}$$

$$h_t^{\mathrm{u,el}} - h_t^{\mathrm{u,fc}} + h_t^{\mathrm{u,dis}} - h_t^{\mathrm{u,ch}} = h_t^{\mathrm{u,in,h}} + h_t^{\mathrm{u,in,g}} - h_t^{\mathrm{u,w,h}}, \quad \forall t \tag{62}$$

$$h_t^{\mathrm{d,el}} - h_t^{\mathrm{d,fc}} + h_t^{\mathrm{d,dis}} - h_t^{\mathrm{d,ch}} = h_t^{\mathrm{d,in,h}} + h_t^{\mathrm{d,in,g}} - h_t^{\mathrm{d,w,h}}, \quad \forall t \tag{63}$$

The amounts of hydrogen injected into the hydrogen grid ($h_t^{\mathrm{i,in,h}}$) or the gas grid ($h_t^{\mathrm{in,g}}$) or withdrawn from the hydrogen grid ($h_t^{\mathrm{i,w,h}}$) are limited by the connection limits – $H^{\mathrm{in,g}}$, $H^{\mathrm{in,h}}$, $H^{\mathrm{w,h}}$, respectively. Injections and withdrawals from the hydrogen system cannot occur at the same time, which is constrained by binary variable $x_t^{\mathrm{i,h}}$. These conditions need to be satisfied in all cases of reserve activation, represented by i.

$$h_t^{\mathrm{i,in,g}} \le H^{\mathrm{in,g}}, \quad \forall t, i \in \{\emptyset, u, d\} \tag{64}$$

$$h_t^{\mathrm{i,in,h}} \le H^{\mathrm{in,h}} \cdot x_t^{\mathrm{i,h}}, \quad \forall t, i \in \{\emptyset, u, d\} \tag{65}$$

$$h_t^{\mathrm{i,w,h}} \le H^{\mathrm{w,h}} \cdot (1 - x_t^{\mathrm{i,h}}), \quad \forall t, i \in \{\emptyset, u, d\} \tag{66}$$

3.4.2. Hydrogen tank constraints

Hydrogen tank constraints are modeled analogously to the ones of the BES. Eqs. (67) and (68) constrain the charging and discharging powers with the installed power of the hydrogen tank. Binary variable $x_t^{\mathrm{i,ht}}$ disable simultaneous charging and discharging. Constraints (67)–(68) need to be valid for the average case of reserve activation, as well as for the highest activation in both directions. SOE of the hydrogen tank (soh_t) is limited by its installed capacity SOH in (69). While the upper and lower limits on the hydrogen tank's SOE must be valid for the highest reserve activation ($i \in \{u, d\}$), as stated in (70), the actual SOE of the hydrogen tank stated in (71) is assumed to change following the average reserve activation ($i = \emptyset$), analogously to the BES constraint (36).

$$h_t^{\mathrm{i,ch}} \le x_t^{\mathrm{i,ht}} \cdot H^{\mathrm{ht}}, \quad \forall t, i \in \{\emptyset, u, d\} \tag{67}$$

$$h_t^{\mathrm{i,dis}} \le (1 - x_t^{\mathrm{i,ht}}) \cdot H^{\mathrm{ht}}, \quad \forall t, i \in \{\emptyset, u, d\} \tag{68}$$

$$0 \le soh_t \le SOH, \quad \forall t \tag{69}$$

$$0 \le soh_{t-1} + (h_t^{\mathrm{i,ch}} - h_t^{\mathrm{i,dis}}) \cdot \Delta t \le SOH, \ \forall t, i \in \{u, d\} \tag{70}$$

$$soh_t = soh_{t-1} + h_t^{\mathrm{ch}} \cdot \Delta t - h_t^{\mathrm{dis}} \cdot \Delta t, \quad \forall t \tag{71}$$

4. Input data

This section provides the main input parameters for the case study. It briefly explains the electrical and hydrogen system assumptions used to obtain the required input data, presents the market, services, and tariffs data, and identifies the installed capacities of all relevant subsystems.

4.1. Electricity system data

Each of the electricity power bus components (PV, BES, electrolyzer, fuel cell) has its own AC/DC converter whose efficiencies are already considered in their overall system efficiencies. The converters are not shown in Figs. 1–3 for simplicity. The modeled electricity power bus voltage is 10 kV. It is transformed to 110 kV in an electrical substation and connected to the high-voltage 110 kV network in Croatia. This transformation is extremely efficient, and its losses are neglected in this paper.

4.2. Hydrogen system data

At the hydrogen bus, the pressures must be harmonized either through compressors (from lower to higher voltage) or through pressure regulators (from higher to lower pressure) [72]. Increasing the pressure requires additional electricity consumption for the compressor operation and its efficiency depends on the inlet and outlet pressure levels. Decreasing the pressures entails only negligible energy losses and we assume this process to be perfectly efficient. Therefore, only the compressors are shown in Figs. 1–3.

The currently available large-scale commercial electrolyzers have hydrogen output pressure 30–40 bars, flexible operation from several percent to 100% of the nominal production rate and startup rate from seconds to 30 min with nominal efficiencies of more than 70%–80% [73–77]. The currently available large-scale commercial fuel cells above 1 MW nominal electric power have hydrogen fuel input pressures 0.55–0.85 bar, flexible operation from several percent to 100% of the nominal production rate and startup rate in the minutes' range and with nominal electrical efficiencies over 50% [72,77,78]. The currently available large-scale commercial hydrogen tanks have pressures 240–1000 bar [76].

The hydrogen bus is modeled as a 50-bar one. The electrolyzers have output hydrogen pressures up to 35 bar, and to increase it to the hydrogen bus level requires further compression. We assume 1.5% energy losses for this compression [38]. The fuel cell needs lower pressure so only the pressure regulator is needed. To store hydrogen in the hydrogen tank (to charge it) a compression to 50 to 350 bar is required and the assumed energy loss for this process is 4% [38]. We model the tank at 350 bar (standard hydrogen tank pressure level). In the discharging mode, only a pressure regulator is needed.

Gas transmission grids in Croatia have pressure levels of 50, 75, and 100 bar. In this paper, we assume a connection to the 50-bar gas grid. The same assumption is made for the hydrogen gas grid (50 bar). When injecting hydrogen into the gas/hydrogen grids, there is no need to further compress. When withdrawing from the hydrogen grid, only the pressure regulator is needed. Therefore, we do not model any energy loss within the hydrogen/gas grid substations.

Electrolyzer and fuel cell coefficients after linearization K_1^{el} and K_2^{el} take values 0.689 and 0.011, while K_1^{fc} and K_2^{fc} take values 2.386 and −0.114, respectively.

Table 1
Characteristic price indices (avg, max and min) at CROPEX during 2019–2021 ($NoNP$ — Number of negative prices).

Value	Year			
	Unit	2019	2020	2021
$\lambda^{\mathrm{da,p}}_{avg}$	€/MWh	42.28	38.01	114.70
$\lambda^{\mathrm{da,p}}_{max}$	€/MWh	200.02	172.07	533.19
$\lambda^{\mathrm{da,p}}_{min}$	€/MWh	−20.23	−23.48	−263.31
$\lambda^{\mathrm{da,g}}_{avg}$	€/MWh	14.72	9.99v	46.63
$\lambda^{\mathrm{da,g}}_{max}$	€/MWh	222.98	17.54	177.40
$\lambda^{\mathrm{da,g}}_{min}$	€/MWh	8.68	4.48	16.00
$\lambda^{\mathrm{da,h}}_{avg}$	€/MWh	–	–	157.22
$\lambda^{\mathrm{da,h}}_{max}$	€/MWh	–	–	637.37
$\lambda^{\mathrm{da,h}}_{min}$	€/MWh	–	–	−5.14
$NoNP$	–	35	27	40

Table 2
Electrical power grid tariffs.

Tariff elements	Units	Power TSO — HOPS	
		Withdrawal	Injection
Energy high tariff	€/MWh	5.33	/
Energy low tariff	€/MWh	2.67	/
Peak power	€/MW	1866.67	170

4.3. Wholesale prices

For the day-ahead prices in this paper we use wholesale electricity prices from the Croatian Power Exchange (CROPEX) [79] for years 2019–2021, natural gas wholesale prices from the Central European Gas Hub (CEGH) for years 2019–2021 [80] and wholesale hydrogen prices as hydrogen index for the year 2021 [64].

Prices in the electricity day-ahead market have changed greatly in the period from 2019 to 2021 and characteristic values are given in Table 1. The year 2020 was marked by a pandemic, due to which the electricity prices fell on average (38.01 €/MWh compared to 42.28 €/MWh in 2019 presents a 10.1% reduction), while the second half of 2021 was marked by a surge in prices about three times compared to the previous two years. The maximum price values share the same characteristics as the average ones, while the minimum value decreased over 10 times in 2021 as compared to 2019 and 2020. The number of periods with negative prices was the highest in 2021. Very similar trends can be observed in the gas day-ahead market prices.

4.4. Grid tariffs

For the grid tariffs, we use the electrical power transmission tariffs for the 110 kV connection by the Croatian Power System Operator HOPS [65], gas transmission tariffs for the 50 bar connection to both the gas and the hydrogen grid by the Croatian Gas Transmission Operator Plinacro [66]. The electrical power grid tariffs are given in Table 2. The electricity element exists for withdrawal direction and is the same all year long. It has the high (07:00–21:00) and the low tariff (21:00–07:00). Peak power is paid for the highest monthly 15-min average power withdrawal/injection.

The gas tariffs are paid for the reserved daily transmission grid capacity in MWh/day and we assume that our reserved daily capacity is equal to the actual gas market trades/grid exchange. The gas tariffs are different for each month and are given in Table 3.

4.5. Balancing capacity, balancing energy and imbalance data

Balancing capacity prices are taken as the automatic frequency restoration reserve (aFRR) capacity price paid to the dominant provider in Croatia in 2021. Balancing energy prices are calculated considering the following rule: for up activation, the TSO pays to the provider 40% on top of the day-ahead price, while for down activation the provider pays to the TSO 40% lower price than the day-ahead price. Similarly, for the up imbalance, the TSO pays to the provider 40% lower price than the day-ahead price, and for the down imbalance, the provider pays to the TSO 40% higher price than the day-ahead price.

Average activated aFRR in both directions is 20% ($A^{\mathrm{u}} = 0.2$, $A^{\mathrm{d}} = 0.2$), average PV forecast error in both directions is 10% ($I^{\mathrm{s}} = 0.1$, $I^{\mathrm{l}} = 0.1$) and to cover it locally at all times we need to reserve 1/(20%) more power capacity in both directions ($A^{\mathrm{u}} = 0.2$, $A^{\mathrm{d}} = 0.2$). Input data for the balancing provision is given in Table 4.

Table 3
Gas grid tariffs.

Months	Units	Gas TSO - Plinacro	
		Withdrawal	Injection
January	€/MWh/day	2.45	4.32
February	€/MWh/day	1.97	3.47
March	€/MWh/day	1.64	2.89
April	€/MWh/day	1.13	1.99
May	€/MWh/day	0.88	1.55
June	€/MWh/day	0.71	1.24
July	€/MWh/day	0.72	1.28
August	€/MWh/day	0.83	1.45
September	€/MWh/day	0.92	1.63
October	€/MWh/day	1.63	2.87
November	€/MWh/day	1.99	3.49
December	€/MWh/day	2.43	4.28

Table 4
Balancing input data.

Parameters	Label	Units	Values
Average up & down reserve activation	$A^{\mathrm{u/d}}$	%	20
Average PV forecast error	$I^{\mathrm{s/l}}$	%	10
aFRR up balancing capacity price	$\lambda^{\mathrm{u,bc}}_t$	€/MW	12.36
aFRR down balancing capacity price	$\lambda^{\mathrm{d,bc}}_t$	€/MW	12.05
aFRR up balancing energy price	$\lambda^{\mathrm{u,be}}_t$	€/MWh	$1.4 \cdot \lambda^{\mathrm{da,p}}_t$
aFRR down balancing energy price	$\lambda^{\mathrm{d,be}}_t$	€/MWh	$0.6 \cdot \lambda^{\mathrm{da,p}}_t$
Up imbalance price	$\lambda^{\mathrm{u,bg}}_t$	€/MWh	$1.4 \cdot \lambda^{\mathrm{da,p}}_t$
Down imbalance price	$\lambda^{\mathrm{d,bg}}_t$	€/MWh	$0.6 \cdot \lambda^{\mathrm{da,p}}_t$

4.6. Installed capacities of the subsystems

The observed facility is primarily a RES power plant with the PV installed electrical power of 100 MW, while the BSS, the electrolyzer, and the fuel cell have installed electrical power of 25, 35, and 11 MW, respectively. Electrical power grid connection limits are 120 MW in the injection and 60 MW in the withdrawal direction. The electrolyzer and the fuel cell have installed hydrogen power of 25 MW. The hydrogen tank charging/discharging hydrogen power limits are 25 MW, while the gas/hydrogen connection limits are 50 MW. Battery energy capacity is 200 MWh (8-hour discharge) with charging/discharging efficiencies 0.86, while the hydrogen tank's energy capacity is 4200 MWh (7-day discharge).

5. Results and discussion

We consider three distinct architectures of the PV-BES-Hydrogen plant introduced in Section 2.1, *HES*, *P2G* and *HES–P2G*, operating in Croatia in the period 2019–2021. Data on the hydrogen index "Hydex" became available only in 2021, which is why the possibility of trading in the hydrogen DAM is considered only in 2021, and such a case is marked as "2021+" . Although the *P2G* and *HES–P2G* models essentially allow trading in that market, it is neglected in 2019 and 2020 due to a lack of data.

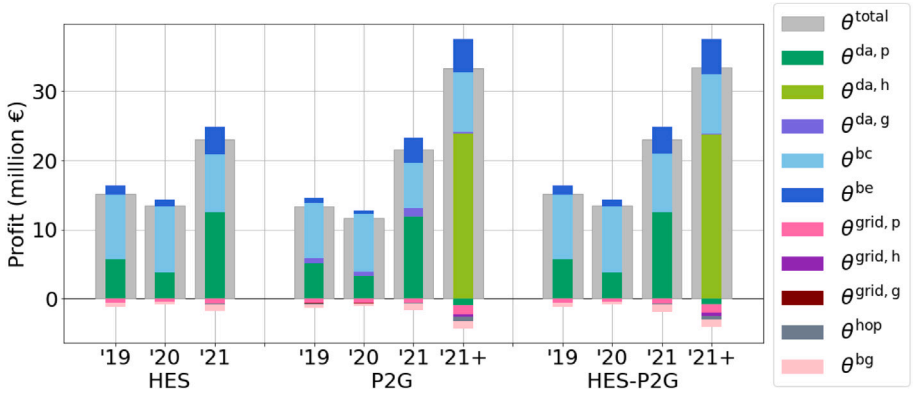

Fig. 6. Profit breakdown during 2019–2021 for all cases.

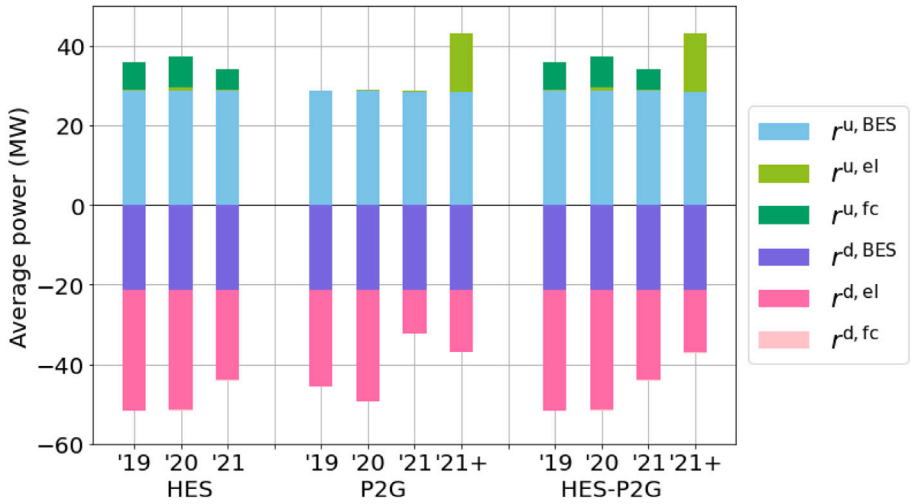

Fig. 7. Average reserve capacity offered by a certain unit during 2019–2021 for all cases.

The results are shown in summarized annual and detailed daily formats. The annual results present the value of different markets, architectures, and subsystems, while the daily results illustrate the behavior of the subsystems. The annual results are shown for all three architectures, while the daily results are only shown only for the *HES-P2G* architecture due to conciseness.

The simulations were performed using Gurobi 9.1.2 run on an AMD Ryzen 7 4700U CPU with 16 GB of RAM at 3733 MHz.

5.1. Hydrogen energy storage — HES results

The *HES* case enables trading in the electricity DAM, along with participating in the balancing service provision and RES BG balancing. Production and exploitation of hydrogen in this case serve exclusively the needs of the power system. First three bars in Figs. 6–8 show profits, average aFRR reserve provision, as well as injected and withdrawn energy, respectively, in the period from 2019 to 2021 for the *HES* case.

Fig. 6 shows the profit breakdown for each year. Each bar consists of the plant's revenues in the positive part and expenditure in the negative part. The highest profit (22.99 million €) is obtained in 2021, due to favorable DAM prices, as seen in Table 1. In comparison to 2019 (15.18 million €), a decrease of 11% in profit is observed in 2020, while 2021 records a significant increase of 51%. The largest portion of the profit comes from the reserved capacity, more precisely 62% in 2019, 70% in 2020, and 36% in 2021.

The average capacity reservation in both directions hardly changes over the years, as seen in Fig. 7, since a constant price is assumed. In 2019, the average reserved capacities were 36.06 MW in the upward and 51.82 MW in the downward direction. A small increase in the value of the average upward reserve provision occurs in 2020 due to low DAM prices, and a decline in the average reserved upward and downward capacities occurred in 2021 when market prices rose sharply in the DAM. Most of the upward reserves in 2019 are provided by the BES (on average 28.77 MW, or 80%), mostly by increasing the discharge (78% of the stated value). The fuel cell on average provides the upward reserve of 7.05 MW (19.54%) by increasing the electricity production. The electrolyzer participates the least in providing the upward reserve, averaging only 0.24 MW in 2019. On the other hand, the downward reserve is mostly provided by the electrolyzer by increasing hydrogen production. It provides an average of 30.46 MW in 2019 (58.78%), while the BES provides 21.20 MW, mostly by increasing the charging (18.73 MW). Only 0.31% is provided by the fuel cell.

In comparison to 2019, there are almost no differences in the average amount of reserves provided in 2020 and its division by units. However, in 2021 the provision of reserves in the downward direction by the electrolyzer decreases (from 30.46 MW to 22.77 MW), due to increased energy prices. Electrolyzer, therefore, works the most in 2020 (98.87% of the year) and in 2021 the least (73.37%). This is the case with the fuel cell as well, which works 89.22% of the time in 2020, and in 2021 only 63.96% of the time. The amount of time periods in

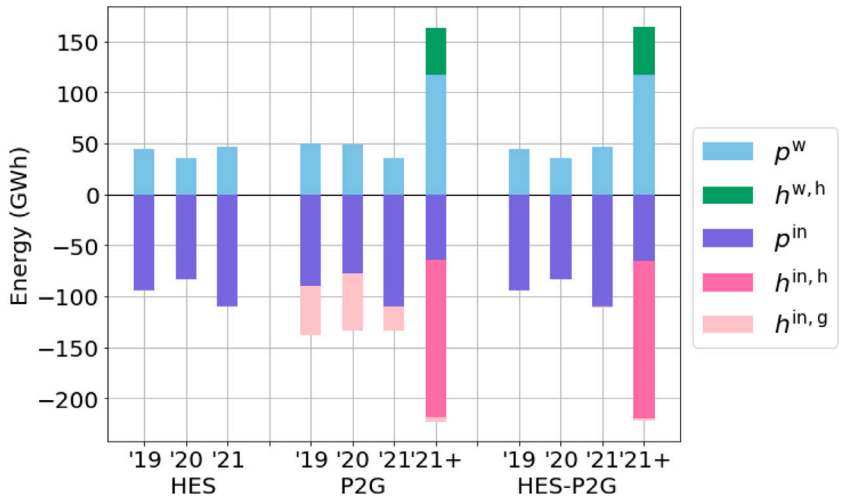

Fig. 8. Withdrawn (positive) and injected (negative) energy from three observed grids during 2019–2021 for all cases.

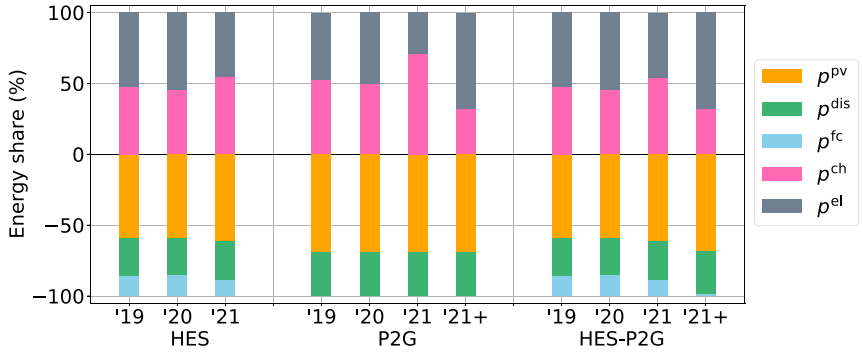

Fig. 9. Breakdown of withdrawn (positive) and injected (negative) electrical energy during 2019–2021 for all cases.

which the electrolyzer operates is higher than that of the fuel cell in all three years. A prerequisite for the fuel cell to work in the HES case is the production of hydrogen from the electrolyzer, which the fuel cell later uses to produce electricity in a more cost-effective period.

The profit share of 37.5% came from the electricity DAM in 2019, which increases to 54.31% in 2021. This increase is mainly due to the disparity in price values, given that the ratio of the purchased and the sold energy in the DAM is similar throughout the years—0.53 (2019), 0.56 (2020), and 0.49 (2021). A profit share of 7%–18%, depending on the year, came from providing BE.

The BES, the electrolyzer, and the fuel cell are never used for BG balancing. Instead, the available capacities are always used to provide reserves. The deviation caused by the PV overproduction can be reduced by increasing the consumption or reducing the production of controllable units. If a surplus remains, it is sold through an imbalance settlement mechanism, but at a price lower than the DAM price as a penalty measure. In spite of the lower imbalance price, the plant still never closes its position before the delivery and the imbalance settlement. In case of the lack of production, the same situation occurs—reserve provision is more profitable than the BG balancing. This occurs in all case studies as negative profits from (not) balancing the BG, see Fig. 6. The plant's profit is further reduced due to the network fees, marked in pink in Fig. 6, whose value is slightly over 3% of the total revenue in all years. Expenditure related to the hydrogen operation equipment is less than 1% of the total plant revenue.

The highest amount of injections into the grid and withdrawals from it happens in 2021, while the lowest in 2020. More precisely, in comparison to 2019, when 94.92 GWh was injected and 44.13 GWh was withdrawn, a decline of 12.77% (injection) and 20.69% (withdrawal) was recorded in 2020 and a surge of 16.36% (injection) and 5.03% (withdrawal) was recorded in 2021, as shown in Fig. 8. The share by the source of withdrawn and injected electricity is shown in detail in Fig. 9. Close to half of the withdrawn electricity annually goes to charging the battery storage, and the rest to operation of the electrolyzer. As for injected energy, approximately 60% of the electricity comes from the PV, 27% from discharging the battery storage, and the rest is produced by the fuel cell.

5.2. Power to gas—P2G results

Besides trading in the electricity DAM, *P2G* allows market trading in the gas and hydrogen DAM.[1] Unlike the *HES* architecture, this case does not model the fuel cell.

Four bars in the middle of Figs. 6–8 represent the results relevant for the *P2G* facility. As in the previous case, the highest profit is realized in the year 2021 (21.53 million €), with a decrease of 6.35% as compared to the *HES* case, as shown in Fig. 6. By far the highest profit is achieved in the year 2021 with the addition of a hydrogen market ("2021+") amounting to 33.28 million € (an increase of 55% when compared to the same year without the hydrogen market).

Fig. 7 shows that the plant provides an average of 28 MW of the upward reserve, exclusively by the BES, in 2019–2021. Since there is no fuel cell, the overall upward reserve capacity is reduced in 2019–2021 as compared to the *HES* case. In the absence of the fuel cell, the operational time of the electrolyzer is significantly decreased as

[1] Hydrogen market is available only in the "2021+" case, so the year 2021 can be compared to the previous years when the hydrogen market did not exist.

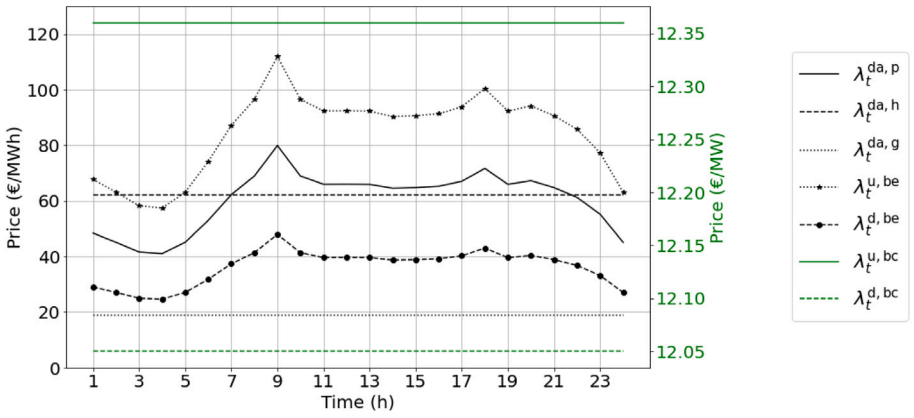

Fig. 10. Prices in all markets on the observed day.

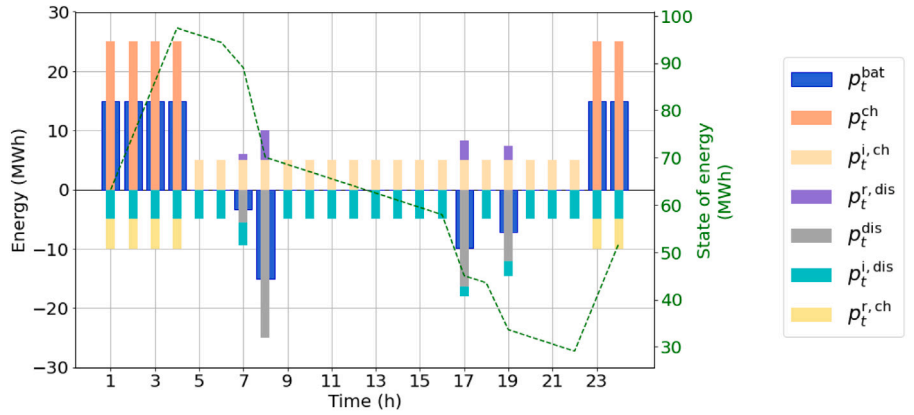

Fig. 11. BES operation on the observed day.

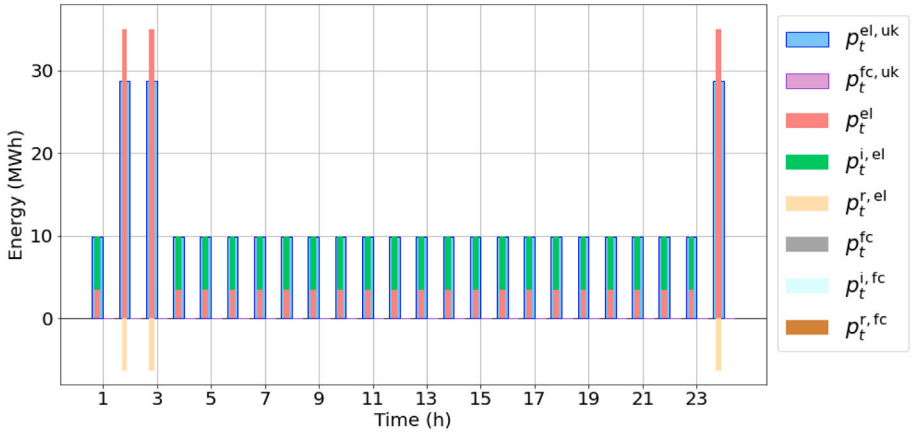

Fig. 12. Electrolyzer and fuel cell operation on the observed day.

compared to the *HES* case to 77.48% of all time periods in 2019, 89.91% in 2020, and 35.65% in 2021. Low DAM prices in 2020 affect both the possibility of arbitrage and the sale of BE, which is why the electrolyzer's operational time in 2020 is higher than in the other two years. On the other hand, high electricity prices in 2021 contribute to a significant reduction in the operation of the electrolyzer. The absence of a fuel cell reduces the need for hydrogen produced from the electrolyzer, and gas market prices compared to electricity prices are not attractive enough for the electrolyzer to produce hydrogen just to sell it in the gas market. As a result, there is less possibility of providing the upward reserve by the electrolyzer and almost all of the upward reserve (over 99%) is provided by the BES.

The same can be observed with the downward reserve. The amount of downward provision by the electrolyzer was reduced due to higher electricity prices, which can especially be seen in the year 2021, in which the average downward reserve provision from the electrolyzer halved from 22.77 MW in the *HES* case to 10.98 MW in the *P2G* case. Specifically, in 2019, total downward average of 45.53 MW is provided (in *HES* 51.82 MW), in 2020 49.41 MW (in *HES* 51.59 MW) and in 2021 32.30 MW (in *HES* 44.13 MW).

When trading in the hydrogen market is enabled ("2021+"), the total yearly operational time of the electrolyzer increases radically from 35.65% to 96.12% of the year. Therefore, the electrolyzer is able to provide more upward reserve (in "2021" it provided 0.18 MW on

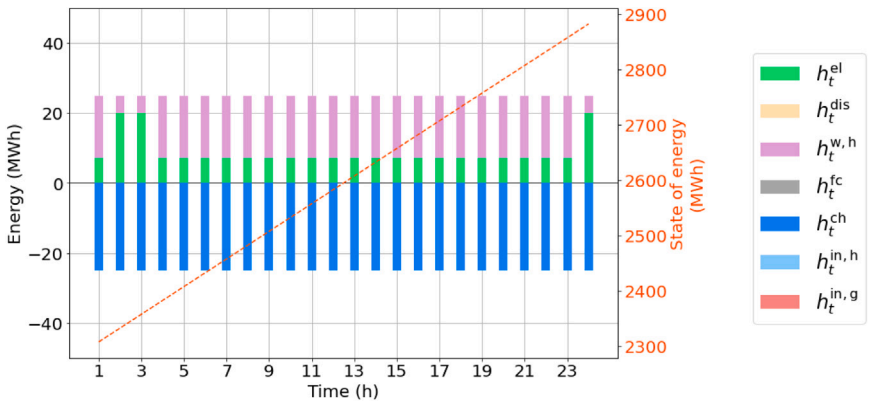

Fig. 13. Hydrogen system operation on the observed day.

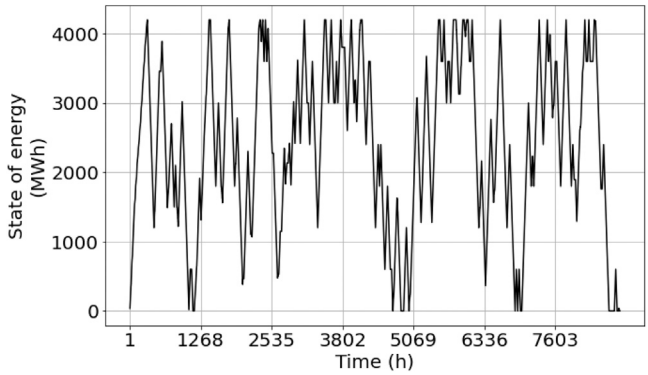

Fig. 14. State-of-energy of the hydrogen tank through the year 2021.

average and in "2021+" 14.51 MW) and therefore the yearly average provision of the upward reserve increases to an average of 43.00 MW in this case, as presented in Fig. 7. Enabling the hydrogen DAM also increases the provision of the downward reserve. As in the *HES* case, the share of profit from the provision of the reserve capacity ranges between 30 and 72%, with the exception of "2021+" where this share decreases to 25% due to the highly profitable hydrogen DAM (see Fig. 6).

The situation in the electricity DAM in the period 2019–2021 is almost the same as in the *HES* case. The electricity purchased for the operation of the electrolyzer is reduced, as well as the sale of the energy produced from the fuel cell, which in this case does not exist. A noticeable change occurs in "2021+" when electricity purchases for the operation of the electrolyzer increase. In this case, the ratio of purchased and sold electricity is 1.43 (in former cases it was around 0.5), resulting in a negative profit from the electricity DAM.

In the period from 2019 to 2021, the hydrogen produced by the electrolyzer is sold in the gas market. Around 5% of the total profit comes from the sale of hydrogen in the gas market (marked purple in between the light-blue and green bars in Fig. 6). On the contrary, in "2021+" the sale of hydrogen in the hydrogen market is more attractive than in the gas market, which can be observed in Table 1. The sale of hydrogen in the gas market occurs in time periods when prices in the hydrogen market are negative, so any positive price in the gas market results in higher revenue as compared to the hydrogen market. Income from the gas market in this case covers 0.61% of the total profit.

Fig. 8 shows the injections and withdrawals from the power, hydrogen, and gas systems. 48.75 GWh is injected into the gas system in 2019, 56.54 GWh in 2020, and 22.84 GWh in 2021. In "2021+", these amounts are reduced to 3.98 GWh injected into the gas system, due to the existence and attractiveness of the hydrogen system. Conversely, 154.70 GWh is injected into the hydrogen system, while 45.85 GWh is withdrawn from it. Lastly, injections to the power grid and withdrawals from it in the *P2G* case are fairly similar to the *HES* case in the period from 2019 to 2021. In the case of "2021+", energy withdrawn from the power system significantly increased to ensure high hydrogen production and its sale to the hydrogen network. In this case, electricity is no longer produced from the fuel cell, and almost 70% of injected electricity comes from the PV (see Fig. 9). Additionally, the electricity for operation of the electrolyzer is increased in the case "2021+" (68%), which was stimulated by the existence of the hydrogen market and attractive prices.

5.3. Hydrogen energy storage + power to gas — HES+P2G annual results

The final case, *HES+P2G*, includes the fuel cell again and allows participation in all markets, i.e. electricity, gas, and hydrogen. Two substudies will be observed for this case: the annual view analogous to the previous two cases (in this chapter), and a daily view to check the unit commitment of the subsystems (the next chapter).

In Figs. 6–8 the rightmost four bars show the results related to this case. For 2019–2021, the results are very similar to the *HES* case. The highest profit of 23 million € is achieved for the year 2021. The only difference is the highly reduced profit in the gas DAM in 2021 (marked purple in between the light-blue and green bars in Fig. 6).

The results for "2021+" are similar to the corresponding ones in the *P2G* case because the fuel cell in the *HES–P2G* case also does not operate much, only 3.74% of the time (the electrolyzer operates 96.24% of the time). Since the fuel cell can use the produced hydrogen when needed, sales in the gas market are avoided when the price is not attractive for sale. Therefore, the profit from the gas DAM reduces to 144,942 € (compared to 203,453 € in the *P2G* case). This can also be seen in Fig. 8, where the injections to the gas grid are barely visible (light pink).

5.4. Hydrogen energy storage + power to gas — HES+ P2G daily results

Since this case involves the interaction of all three DAMs and all controllable units, we present the results for this case on a specific day in Figs. 11–12.

5.4.1. Battery energy storage operation

Fig. 11 shows the BES operation on an observed day. The total discharged energy from or charged to the BES is shown in a wider blue bar for each time period. Other bars represent the energies used for the DAM charging and BE provision according to the variables from Section 3. In addition, SOE of the BES (dashed green line, secondary y-axis) is shown. To better explain the reasons for a certain behavior, prices during the observed day are provided in Fig. 10 for all considered markets.

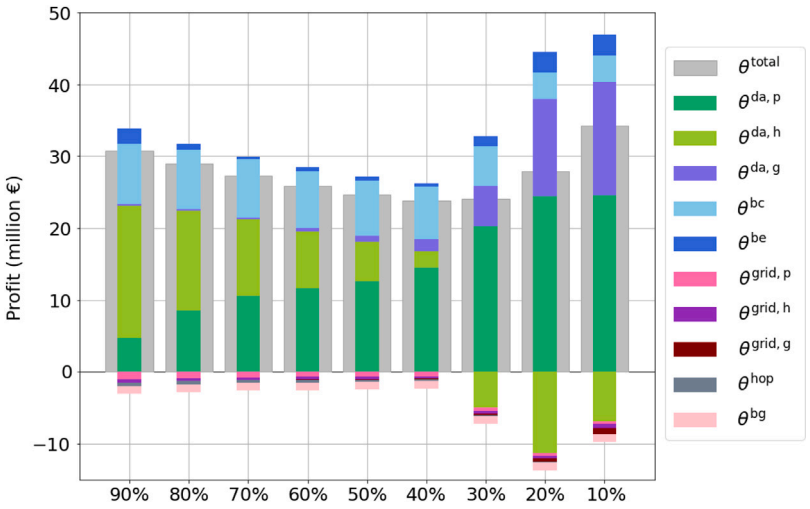

Fig. 15. Profit breakdown for *HES+P2G* in case of hydrogen prices' decline to [10%, 90%] of their initial value.

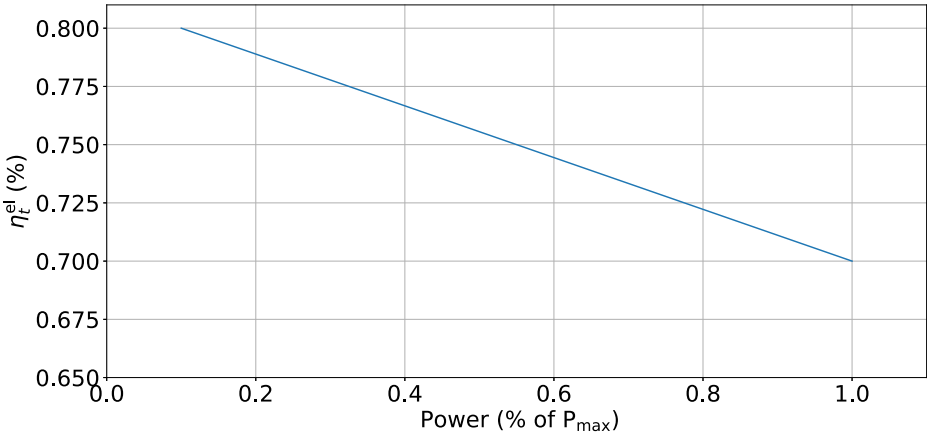

Fig. 16. Electrolyzer efficiency dependent on its operation power.

Time periods of low prices in the electricity DAM occur at the beginning (hours 1–4) and end (hours 23 and 24) of the day. Therefore, the BES charges in these periods (light gray bars on the positive y-axis). The BES is charged at maximum power of 25 MW at these times. Along with participating in the DAM, the BES also provides upward reserve during those hours. To take into account the uncertainty of reserve provision, the model is designed so that the reserved upward and downward capacities must meet constraints (34) and (35), and only a certain share of BC ($A^{u/d}$) is activated in the form of BE in real-time. During the period when the BES is being charged at maximum power, it also reserves the capacity to provide upward reserve and activates a portion of it (shown in Fig. 11). The upward reserve is provided by increasing the discharging power and/or by reducing the charging power. Since the BES is charging at maximum power, it is possible to reserve a total capacity of double the maximum power of the BES. It first reduces the charging power to zero and then increases the discharge to the maximum power.

During periods of high prices (e.g. hour 8), the BES is discharged and the same situation as previously explained, but in the opposite direction occurs, this time with the downward reserves. The dashed green curve in Fig. 11 shows the SOE of the BES, which changes depending on the energy that was actually charged to or discharged from the BES in a certain time period (wide blue bars).

5.4.2. Fuel cell and electrolyzer power operation

The operation of the fuel cell and the electrolyzer is shown in Fig. 12. The electrolyzer operation is noted on the positive *y*-axis and the fuel cell on the negative *y*-axis. The total energy purchased for the operation of the electrolyzer or sold upon its generation in the fuel cell is given in a wider bar for each time period—blue for the electrolyzer and pink for the fuel cell. The other bars represent the day-ahead scheduled energy and activated balancing energy according to the variables from Section 3

Most electricity needed for the operation of the electrolyzer is purchased in low-price time periods in the DAM (hours 2, 3, and 24). Just as with the BES, the capacity required to provide the BC in the maximum possible amount is reserved (it is necessary to take into account the technical minimum of the fuel cell and the electrolyzer). This is achieved by reducing the electrolyzer's operation to its technical minimum. The total electricity used for the operation of the electrolyzer is shown with wide blue bars, as the difference between the energy purchased in the DAM and the BE delivered by the electrolyzer. On an observed day, the fuel cell did not operate.

5.4.3. Hydrogen busbar operation

The effect of the electrolyzer operation, shown in Fig. 12, on the hydrogen system is presented in Fig. 13. It presents the hydrogen injections and withdrawals, which is why the sum of positive (hydrogen production and purchase, hydrogen tank discharging) and negative energy (charging the hydrogen into the tank, hydrogen for fuel cell operation, hydrogen injected into hydrogen and gas grid) is zero at all time periods.

In hours 2, 3, and 24, when more electricity is consumed for the electrolyzer operation, more hydrogen (green bars) is produced.

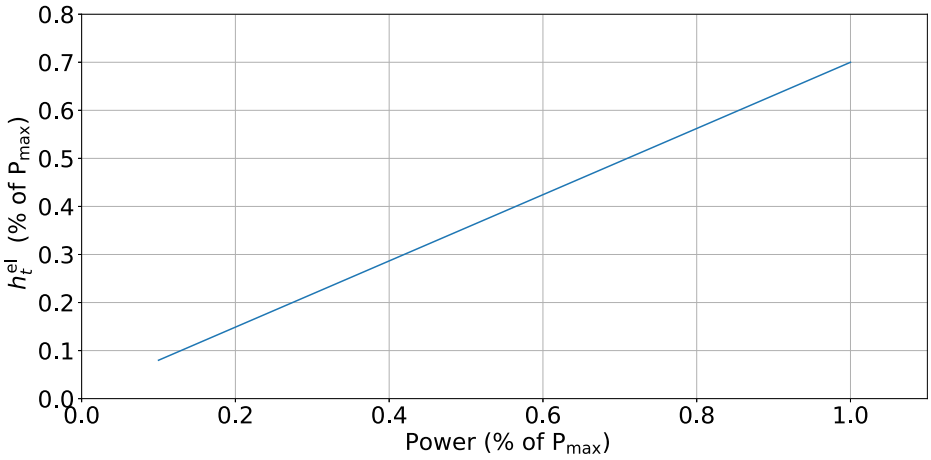

Fig. 17. Produced hydrogen in power units vs electrolyzer operation power.

During the shown 24-hour period, the price in the hydrogen DAM was low, thus, it was used to buy hydrogen (purple bars). The purchased hydrogen, as well as the one produced by the electrolyzer, is filled into the hydrogen tank at maximum power so it can be later sold at a higher price. The hydrogen DAM price during the day is fixed, and the differences in prices can be seen only between days. According to the price difference between different days, the tank is filled or emptied constantly throughout the day. On an observed day, the price is low and the hydrogen tank is charged during all hours.

The behavior of the tank throughout the year is presented in Fig. 14. The tank performs an inter-day arbitrage and cycles throughout the year, making it a multi-day or seasonal energy storage. The seasonal effect on the hydrogen tank operation is driven predominantly by the variable hydrogen DAM price, i.e. the tank charges when the prices are at a local minima, and the tank discharges when the price are at a local maxima. The local minima and maxima in this context appear every few days or weeks. However, other seasonal inputs affect the operation of hydrogen tank as well. For example, a low electricity DAM price increases operation of the fuel cell and therefore charging of the hydrogen tank and, vice versa, during low prices, high PV production results in excess of electricity which can be used for electrolysis.

5.5. Hydrogen energy storage + power to gas — HES+P2G sensitivity analysis on future hydrogen prices

To investigate how would an RES-BES-Hydrogen plant behave in the event of an expected hydrogen DAM price decrease, we present an additional sensitivity analysis using different percentage of the hydrogen price decrease. Simulations were run for hydrogen prices reductions to [10%,90%] of their initial value. Fig. 15 shows how the profit changes for different hydrogen prices expected in the future. While the prices above 40% of their initial value, the overall profit declines. It is not as profitable to buy electricity for the electrolyzer operation and to sell it in the hydrogen DAM as it is at the initial prices. After a further decline to 30% of the initial value, the price in the hydrogen DAM is attractive enough to purchase hydrogen and to sell it in the gas DAM, which can be seen as an increasing purple part of the bars and an increasing negative part in light green. However, at 30% of the initial value, the average price in the hydrogen DAM is still higher than the average price in the gas DAM, therefore only after another 10% decline does the profit in the gas DAM increase significantly. Along with the increase in profit from sales in the gas DAM, the profit in the electricity DAM also increases because the yearly operation time of the fuel cell increases from 64% (at 30% of the initial value) to over 90% in the last two cases of price reduction.

To sum up, the decline in the hydrogen DAM price in the first phase results in a decline in revenues arising from hydrogen sales in the DAM, but it is also characterized by the revenue increase due to the electricity DAM sales. The electricity DAM revenues increase is lower than the decrease in revenues from the hydrogen DAM, thus the total profit decreases. In the second phase, after the hydrogen and natural gas price parity is reached, the increase in the electricity DAM revenues continues, but it is coupled with significant revenues from gas DAM, and the overall profit increases.

6. Conclusion

The paper discusses three architectures of the PV–battery-hydrogen plants that differ in the possibility of participating in the gas and hydrogen markets and in the existence of a fuel cell, presented in the paper as the *HES*, *P2G* and *HES–P2G* cases. In all these cases and throughout almost all the observed years, the highest share of profit comes from providing BC. The exception is the case when trading in the hydrogen market is enabled ("2021+"), which becomes the most profitable trading floor. Since the hydrogen DAM is at a very early stage of adoption, we provided a sensitivity analysis using different hydrogen DAM prices to take into account its uncertain evolution. This analysis indicates that lowering the hydrogen DAM price (which is expected) will significantly change the profit breakdown of the proposed facility from mostly hydrogen DAM sales to electricity and gas sales.

In all cases, the BES is mostly used to provide reserves to the power system. The fuel cell and the electrolyzer in the *HES* case operate for more than half-time periods of the year and also take part in providing reserves. The electrolyzer largely provides the downward reserve by increasing its hydrogen production, and the fuel cell provides the upward reserve by increasing its electricity production. In the absence of the fuel cell and with the trading being allowed only in the gas and power markets, i.e. the *P2G* case, the electrolyzer significantly reduces its total yearly operational time to just over a third of the year. Conversely, in the case when trading in the hydrogen market is also enabled, the operating time of the electrolyzer is increased to almost the entire year, and the upward reserve provision is increased as well. When the fuel cell operation is additionally enabled in the previously described case (*HES–P2G*), the results do not change significantly since it operates for less than 5% of the year. The BES, the electrolyzer, and the fuel cell do not provide any BG deviation balancing services in all the observed cases. In other words, under current Croatian prices, it is more profitable to provide balancing services to the TSO than to balance its own imbalances. Finally, the BES and the hydrogen tank perform arbitrage in the DAM, with the BES optimizing its operation on an hourly basis (short-term) and the hydrogen tank on a daily basis (medium to long-term).

In our future work we will focus on two directions: integration of uncertainty of input parameters to create more accurate daily operational algorithms and investigation of seasonality effect on operation of different devices within the facility.

CRediT authorship contribution statement

Ivan Pavić: Conceptualization, Data curation, Methodology, Visualisation, Investigation, Writing – original draft. **Nikolina Čović:** Conceptualization, Formal analysis, Software, Visualisation, Investigation, Writing – original draft. **Hrvoje Pandžić:** Resources, Writing – review & editing, Supervision, Funding acquisition.

Declaration of competing interest

The authors declare that they have no known competing financial interests or personal relationships that could have appeared to influence the work reported in this paper.

Data availability

Data will be made available on request.

Acknowledgments

This work was supported by the Croatian Science Foundation and the European Union through the European Social Fund under project Flexibility of Converter-based Microgrids – FLEXIBASE (PZS-2019-02-7747).

Appendix

The efficiency of an electrolyzer depends on its operating power. The linearized curve of this dependence is shown in Fig. 16. Thus, at $10\% \cdot P^{\mathrm{el}}$ the efficiency is 80%, and at maximal power it is 70% [73–77]. However, (49) models a nonlinear relationship that needs to be linearized for the problem to be solved by linear programming. Therefore, dependence of h_t^{el} (49) on $p_t^{\mathrm{ee,el}}$ is modeled. The equation of the line shown in Fig. 17, (50), is used as the final constraint used instead of (49). The same procedure is done in the case of fuel cell, with 41% efficiency at $10\% \cdot P^{\mathrm{fc}}$ and 32% at P^{fc} [69].

References

[1] EU Commission. Communication from the commission to the European parliament, the European council, the council, the European economic and social committee and the committee Of The Regions the European green deal COM/2019/640 final. 2019, URL https://eur-lex.europa.eu/legal-content/EN/TXT/?uri=CELEX:52019DC0640.

[2] Eurostat. Renewable energy statistics. 2020, URL https://ec.europa.eu/eurostat/statistics-explained/index.php?title=Renewable_energy_statistics#Share_of_renewable_energy_more_than_doubled_between_2004_and_2019.

[3] Koivisto M, Sørensen P, Maule P, Nuño Martinez E. Needs for flexibility caused by the variability and uncertainty in wind and solar generation in 2020, 2030 and 2050 scenarios. Denmark: DTU Wind Energy; 2017.

[4] Impram S, Nese SV, Oral B. Challenges of renewable energy penetration on power system flexibility: A survey. Energy Strategy Rev 2020;31:100539. http://dx.doi.org/10.1016/J.ESR.2020.100539.

[5] Miletić M, Luburić Z, Pavić I, Capuder T, Pandžić H, Andročec I, Marušić A. A review of energy storage systems applications. In: Mediterranean conference on power generation, transmission, distribution and energy conversion (MEDPOWER 2018). 2018, p. 1–6. http://dx.doi.org/10.1049/cp.2018.1926.

[6] International Renewable Energy Agency. Utility scale batteries. Tech. rep., International Renewable Energy Agency; 2019, URL /newsroom/articles/2020/Mar/Battery-storage-paves-way-for-a-renewable-powered-future.

[7] Bobanac V, Bašić H, Pandžić H. Determining lithium-ion battery one-way energy efficiencies: Influence of C-rate and coulombic losses. In: EUROCON 2021 - 19th IEEE international conference on smart technologies, proceedings. Institute of Electrical and Electronics Engineers Inc.; 2021, p. 385–9. http://dx.doi.org/10.1109/EUROCON52738.2021.9535542.

[8] Penev M, Hunter C, Eichman JD. Energy storage: Days of service sensitivity analysis. 2019, URL https://www.osti.gov/biblio/1507686.

[9] Bowen T, Chernyakhovskiy I, Xu K, Gadzanku S, Coney K. Usaid grid-scale energy storage technologies primer. Tech. rep., NREL; 2021, URL www.nrel.gov/publications.

[10] Wind Europe. Wind energy and on-site energy storage. Tech. rep., Wind Europe; 2017, URL https://windeurope.org/wp-content/uploads/files/policy/position-papers/WindEurope-Wind-energy-and-on-site-energy-storage.pdf.

[11] Gevorgian V, Wallen R, Koralewicz P, Mendiola E, Shah S, Morjaria M. Provision of Grid Services by PV Plants with Integrated Battery Energy Storage System: Preprint. Tech. rep., NREL; 2020, URL www.nrel.gov/publications.

[12] Keerthisinghe C, Mickelson E, Kirschen DS, Shih N, Gibson S. Improved PV forecasts for capacity firming. IEEE Access 2020;8:152173–82. http://dx.doi.org/10.1109/ACCESS.2020.3016956.

[13] Liu M, Quilumba FL, Lee WJ. Dispatch scheduling for a wind farm with hybrid energy storage based on wind and LMP forecasting. IEEE Trans Ind Appl 2015;51(3):1970–7. http://dx.doi.org/10.1109/TIA.2014.2372043.

[14] Małkowski R, Jaskólski M, Pawlicki W. Operation of the hybrid photovoltaic-battery system on the electricity Market—Simulation, real-time tests and cost analysis. Energies 2020;13(6):1402. http://dx.doi.org/10.3390/EN13061402, https://www.mdpi.com/1996-1073/13/6/1402/htmhttps://www.mdpi.com/1996-1073/13/6/1402.

[15] Chakir A, Tabaa M, Moutaouakkil F, Medromi H, Julien-Salame M, Dandache A, Alami K. Optimal energy management for a grid connected PV-battery system. Energy Rep 2020;6:218–31. http://dx.doi.org/10.1016/J.EGYR.2019.10.040.

[16] Yi Z, Dong W, Etemadi AH. A unified control and power management scheme for PV-Battery-based hybrid microgrids for both grid-connected and islanded modes. IEEE Trans Smart Grid 2018;9(6):5975–85. http://dx.doi.org/10.1109/TSG.2017.2700332.

[17] Hasanpor Divshali P, Evens C. Optimum operation of battery storage system in frequency containment reserves markets. IEEE Trans Smart Grid 2020;11(6):4906–15. http://dx.doi.org/10.1109/TSG.2020.2997924.

[18] Nitsch F, Deissenroth-Uhrig M, Schimeczek C, Bertsch V. Economic evaluation of battery storage systems bidding on day-ahead and automatic frequency restoration reserves markets. Appl Energy 2021;298:117267. http://dx.doi.org/10.1016/J.APENERGY.2021.117267.

[19] Angenendt G, Merten M, Zurmühlen S, Sauer DU. Evaluation of the effects of frequency restoration reserves market participation with photovoltaic battery energy storage systems and power-to-heat coupling. Appl Energy 2020;260:114186. http://dx.doi.org/10.1016/J.APENERGY.2019.114186.

[20] Conte F, Massucco S, Schiapparelli GP, Silvestro F. Day-ahead and intra-day planning of integrated BESS-PV systems providing frequency regulation. IEEE Trans Sustain Energy 2020;11(3):1797–806. http://dx.doi.org/10.1109/TSTE.2019.2941369.

[21] He G, Chen Q, Kang C, Pinson P, Xia Q. Optimal bidding strategy of battery storage in power markets considering performance-based regulation and battery cycle life. IEEE Trans Smart Grid 2016;7(5):2359–67. http://dx.doi.org/10.1109/TSG.2015.2424314.

[22] Zobaa A, Ribeiro P, Aleem SA, Afifi S. Energy storage at different voltage levels: Technology, integration, and market aspects. Herts, United Kingdom: The Institution of Engineering and Technology – IET; 2018, http://dx.doi.org/10.17226/10922, URL https://shop.theiet.org/energy-storage-at-differ-1e.

[23] Čović N, Braeuer F, McKenna R, Pandžić H. Optimal PV and battery investment of market-participating industry facilities. IEEE Trans Power Syst 2021;36(4):3441–52. http://dx.doi.org/10.1109/TPWRS.2020.3047260.

[24] Hanif S, Alam MJ, Roshan K, Bhatti BA, Bedoya JC. Multi-service battery energy storage system optimization and control. Appl Energy 2022;311:118614. http://dx.doi.org/10.1016/J.APENERGY.2022.118614.

[25] Huang B, Wang J. Deep-reinforcement-learning-based capacity scheduling for PV-battery storage system. IEEE Trans Smart Grid 2021;12(3):2272–83. http://dx.doi.org/10.1109/TSG.2020.3047890.

[26] Almasalma H, Deconinck G. Simultaneous provision of voltage and frequency control by PV-battery systems. IEEE Access 2020;8:152820–36. http://dx.doi.org/10.1109/ACCESS.2020.3018086.

[27] Islam MS, Mithulananthan N, Lee KY. Suitability of PV and battery storage in EV charging at business premises. IEEE Trans Power Syst 2018;33(4):4382–96. http://dx.doi.org/10.1109/TPWRS.2017.2774361.

[28] Li S, Zhu J, Dong H, Zhu H, Fan J. A novel rolling optimization strategy considering grid-connected power fluctuations smoothing for renewable energy microgrids. Appl Energy 2022;309:118441. http://dx.doi.org/10.1016/J.APENERGY.2021.118441.

[29] Narayanan V, Kewat S, Singh B. Solar PV-BES based microgrid system with multifunctional VSC. IEEE Trans Ind Appl 2020;56(3):2957–67. http://dx.doi.org/10.1109/TIA.2020.2979151.

[30] Xia Y, Yu M, Yang P, Peng Y, Wei W. Generation-storage coordination for Islanded DC microgrids dominated by PV generators. IEEE Trans Energy Convers 2019;34(1):130–8. http://dx.doi.org/10.1109/TEC.2018.2860247.

[31] Fatin Ishraque M, Shezan SA, Ali MM, Rashid MM. Optimization of load dispatch strategies for an islanded microgrid connected with renewable energy sources. Appl Energy 2021;292:116879. http://dx.doi.org/10.1016/J.APENERGY.2021.116879.

[32] Zhang B, Dehghanian P, Kezunovic M. Optimal allocation of PV generation and battery storage for enhanced resilience. IEEE Trans Smart Grid 2019;10(1):535–45. http://dx.doi.org/10.1109/TSG.2017.2747136.

[33] Li J, You H, Qi J, Kong M, Zhang S, Zhang H. Stratified optimization strategy used for restoration with photovoltaic-battery energy storage systems as black-start resources. IEEE Access 2019;7:127339–52. http://dx.doi.org/10.1109/ACCESS.2019.2937833.

[34] Pavić I, Luburić Z, Pandžić H, Capuder T, Andročec I. Defining and evaluating use cases for battery energy storage investments: Case study in Croatia. Energies 2019;12:376. http://dx.doi.org/10.3390/EN12030376, https://www.mdpi.com/1996-1073/12/3/376/htmhttps://www.mdpi.com/1996-1073/12/3/376.

[35] Luburić Z, Pandžić H, Plavšić T, Teklić L, Valentić V. Role of energy storage in ensuring transmission system adequacy and security. Energy 2018;156:229–39. http://dx.doi.org/10.1016/J.ENERGY.2018.05.098.

[36] El-Shafie M, Kambara S, Hayakawa Y, El-Shafie M, Kambara S, Hayakawa Y. Hydrogen production technologies overview. J Power Energy Eng 2019;7:107–54. http://dx.doi.org/10.4236/JPEE.2019.71007, http://www.scirp.org/journal/PaperInformation.aspx?PaperID=90227http://www.scirp.org/Journal/Paperabs.aspx?paperid=90227.

[37] International Energy Agency. The Future of Hydrogen. Tech. rep., 2019, https://iea.blob.core.windows.net/assets/9e3a3493-b9a6-4b7d-b499-7ca48e357561/The_Future_of_Hydrogen.pdf URL https://www.iea.org/reports/the-future-of-hydrogen.

[38] Elberry AM, Thakur J, Santasalo-Aarnio A, Larmi M. Large-scale compressed hydrogen storage as part of renewable electricity storage systems. Int J Hydrogen Energy 2021;46(29):15671–90. http://dx.doi.org/10.1016/J.IJHYDENE.2021.02.080.

[39] Gerwen RV, Eijgelaar M, Bosma T. The promise of seasonal storage. Tech. rep., DNV GL; 2020.

[40] Advisory G, Consulting AA. Hydrogen to support electricity systems. Tech. rep., (May):GHD Advisory and ACIL Allen Consulting; 2020, p. 105.

[41] Alshehri F, Suárez VG, Rueda Torres JL, Perilla A, van der Meijden MA. Modelling and evaluation of PEM hydrogen technologies for frequency ancillary services in future multi-energy sustainable power systems. Heliyon 2019;5(4):e01396. http://dx.doi.org/10.1016/J.HELIYON.2019.E01396.

[42] Dozein MG, Jalali A, Mancarella P. Fast frequency response from utility-scale hydrogen electrolyzers. IEEE Trans Sustain Energy 2021;12(3):1707–17. http://dx.doi.org/10.1109/TSTE.2021.3063245.

[43] Gao D, Jiang D, Liu P, Li Z, Hu S, Xu H. An integrated energy storage system based on hydrogen storage: Process configuration and case studies with wind power. Energy 2014;66:332–41. http://dx.doi.org/10.1016/J.ENERGY.2014.01.095.

[44] Komiyama R, Otsuki T, Fujii Y. Energy modeling and analysis for optimal grid integration of large-scale variable renewables using hydrogen storage in Japan. Energy 2015;81:537–55. http://dx.doi.org/10.1016/J.ENERGY.2014.12.069.

[45] Mayyas A, Wei M, Levis G. Hydrogen as a long-term, large-scale energy storage solution when coupled with renewable energy sources or grids with dynamic electricity pricing schemes. Int J Hydrogen Energy 2020;45(33):16311–25. http://dx.doi.org/10.1016/J.IJHYDENE.2020.04.163.

[46] Guerra OJ, Zhang J, Eichman J, Denholm P, Kurtz J, Hodge B-M. The value of seasonal energy storage technologies for the integration of wind and solar power. Energy Environ Sci 2020;13(7):1909–22. http://dx.doi.org/10.1039/D0EE00771D, https://pubs.rsc.org/en/content/articlehtml/2020/ee/d0ee00771dhttps://pubs.rsc.org/en/content/articlelanding/2020/ee/d0ee00771d.

[47] European Commission. Communication from the commission to the European parliament, the council, the European economic and social committee and the committee of the regions a hydrogen strategy for a climate-neutral Europe Europe. 2020, URL https://www.eu2018.at/calendar-events/political-events/BMNT-.

[48] European Commission. A hydrogen strategy for a climate-neutral Europe. 2020, URL https://www.eu2018.at/calendar-events/political-events/BMNT-.

[49] Department for Business, Energy & Industrial Strategy U. Hydrogen Production Costs 2021. Tech. Rep., (August). Department for Business, Energy & Industrial Strategy, UK; 2021, URL https://www.iea.org/data-and-statistics/charts/hydrogen-production-costs-by-production-source-2018.

[50] ICCT. Assessment of hydrogen production costs from electrolysis: United states and Europe. International Council on Clean Transportation (ICCT); 2020, p. 1–73, URL https://theicct.org/sites/default/files/publications/final{_}icct2020{_}assessment{_}of{_}hydrogen{_}production{_}costsv2.pdf.

[51] Wang A, Jens J, Mavins D, Moultak M, Schimmel M, Leun KVD, Peters D, Buseman M. Analysing future demand, supply, and transport of hydrogen: European hydrogen backbone. 2021, URL https://transparency.entsog.eu/.

[52] of Transmission System Operators for Gas EN. Entsog 2050 roadmap for gas grids. 2019, URL www.entsog.eu.

[53] PwC. HyWay 27 : hydrogen transmission using the existing natural gas grid ? final report for the ministry of economic affairs and climate policy. Tech. Rep, (June). Amsterdam: PwC/Strategy&; 2021.

[54] Götz M, Lefebvre J, Mörs F, McDaniel Koch A, Graf F, Bajohr S, Reimert R, Kolb T. Renewable Power-to-Gas: A technological and economic review. Renew Energy 2016;85:1371–90. http://dx.doi.org/10.1016/J.RENENE.2015.07.066.

[55] Schiebahn S, Grube T, Robinius M, Tietze V, Kumar B, Stolten D. Power to gas: Technological overview, systems analysis and economic assessment for a case study in Germany. Int J Hydrogen Energy 2015;40(12):4285–94. http://dx.doi.org/10.1016/J.IJHYDENE.2015.01.123.

[56] Janke L, McDonagh S, Weinrich S, Murphy J, Nilsson D, Hansson PA, Nordberg A. Optimizing power-to-H2 participation in the Nord Pool electricity market: Effects of different bidding strategies on plant operation. Renew Energy 2020;156:820–36. http://dx.doi.org/10.1016/J.RENENE.2020.04.080.

[57] Zhang R, Jiang T, Li F, Li G, Chen H, Li X. Coordinated bidding strategy of wind farms and power-to-gas facilities using a cooperative game approach. IEEE Trans Sustain Energy 2020;11(4):2545–55.

[58] Pan G, Gu W, Lu Y, Qiu H, Lu S, Yao S. Accurate modeling of a profit-driven power to hydrogen and methane plant toward strategic bidding within multi-type markets. IEEE Trans Smart Grid 2021;12(1):338–49. http://dx.doi.org/10.1109/TSG.2020.3019043.

[59] Li X, Mulder M. Value of power-to-gas as a flexibility option in integrated electricity and hydrogen markets. Appl Energy 2021;304:117863. http://dx.doi.org/10.1016/J.APENERGY.2021.117863.

[60] Pongrašić M, Tomšić Željko. Cost-benefit analysis of smart grid projects implementation. J Energy (Energ) 2017;66:87–98. http://dx.doi.org/10.37798/EN2017661-497, URL http://www.journalofenergy.com/index.php/joe/article/view/97/73.

[61] ENTSO-E. ENTSO-E Market Report 2020. Tech. rep., 2020.

[62] ACER/CEER. Annual report on the results of monitoring the internal electricity and natural gas markets in 2020 gas wholesale markets volume. 2021.

[63] den Ouden B. A hydrogen exchange for the climate. Tech. rep., Amsterdam; 2020, p. 1–23, URL https://www.government.nl/binaries/government/documents/reports/2020/09/24/a-hydrogen-exchange-for-the-climate/A+Hydrogen+exchange+for+the+Climate.pdf.

[64] S&P Global Platts. Latest oil, energy & metals news, market data and analysis. 2021, URL https://www.spglobal.com/platts/en.

[65] Croatian Transmission System Operator. HOPS. 2021, URL https://www.hops.hr/.

[66] Croatian Gas Transmission System Operator. PLINACRO d.o.o.. 2021, URL https://www.plinacro.hr/.

[67] Pandžić H, Bobanac V. An accurate charging model of battery energy storage. IEEE Trans Power Syst 2019;34(2):1416–26. http://dx.doi.org/10.1109/TPWRS.2018.2876466.

[68] Global hydrogen review 2021. Tech. rep., IEA; 2021.

[69] San Martín JI, Zamora I, Asensio FJ, García-Villalobos J, San Martín JJ, Aperribay V. Control and management of a fuel cell microgrid. Energy efficiency optimization. Renew Energy Power Qual J 2013;1(11):314–9. http://dx.doi.org/10.24084/REPQJ11.290.

[70] Chauvin A, Sari A, Hijazi A, Bideaux E. Optimal sizing of an energy storage system for a hybrid vehicle applied to an off-road application. In: IEEE/ASME international conference on advanced intelligent mechatronics, AIM. Institute of Electrical and Electronics Engineers Inc.; 2014, p. 775–80. http://dx.doi.org/10.1109/AIM.2014.6878173.

[71] Rafique MK, Haider ZM, Mehmood KK, Uz Zaman MS, Irfan M, Khan SU, Kim CH. Optimal scheduling of hybrid energy resources for a smart home. Energies 2018;11(11). http://dx.doi.org/10.3390/EN11113201.

[72] Barbir F. Fuel cell system design. Academic Press; 2013, p. 305–72. http://dx.doi.org/10.1016/B978-0-12-387710-9.00009-6.

[73] ITM Power. HGas3SP | ITM power. 2021, URL https://itm-power.com/products/hgas3sp.

[74] Enapter. AEM multicore - green hydrogen at megawatt scale - enapter. 2021, URL https://enapter.com/aem-multicore/.

[75] H-Tec Systems. PEM electrolyser ME450/1400: H-TEC SYSTEMS products. 2021, URL https://www.h-tec.com/en/products/detail/h-tec-pem-electrolyser-me450-1400/me450-1400/.

[76] Nel. Containerized PEM electrolyser | nel hydrogen. 2021, URL https://nelhydrogen.com/product/m-series-containerized/.

[77] Plug Power. Plug power | green hydrogen & fuel cell solutions. 2021, URL https://www.plugpower.com/.

[78] Toshiba-energy. Pure hydrogen fuel cell system H2rex. 2021, URL https://www.toshiba-energy.com/en/hydrogen/product/fuel-cell.htm.

[79] Croatian Power Exchange. Hrvatska burza električne energije. 2021, URL https://www.cropex.hr/hr/.

[80] Central European Gas Hub. Home | CEGH. 2021, URL https://www.cegh.at/.